J Biol Inorg Chem (2016) 21:619–644
DOI 10.1007/s00775-016-1357-8

MINIREVIEW

Mono- and binuclear non-heme iron chemistry from a theoretical perspective

Tibor András Rokob[3] · Jakub Chalupský[1] · Daniel Bím[1] · Prokopis C. Andrikopoulos[1] · Martin Srnec[2] · Lubomír Rulíšek[1]

Received: 4 March 2016 / Accepted: 29 April 2016 / Published online: 26 May 2016

Abstract In this minireview, we provide an account of the current state-of-the-art developments in the area of mono- and binuclear non-heme enzymes (NHFe and $NHFe_2$) and the smaller $NHFe_{(2)}$ synthetic models, mostly from a theoretical and computational perspective. The sheer complexity, and at the same time the beauty, of the $NHFe_{(2)}$ world represents a challenge for experimental as well as theoretical methods. We emphasize that the concerted progress on both theoretical and experimental side is a *conditio sine qua non* for future understanding, exploration and utilization of the $NHFe_{(2)}$ systems. After briefly discussing the current challenges and advances in the computational methodology, we review the recent spectroscopic and computational studies of $NHFe_{(2)}$ enzymatic and inorganic systems and highlight the correlations between various experimental data (spectroscopic, kinetic, thermodynamic, electrochemical) and computations. Throughout, we attempt to keep in mind the most fascinating and attractive phenomenon in the $NHFe_{(2)}$ chemistry, which is the fact that despite the strong oxidative power of many reactive intermediates, the $NHFe_{(2)}$ enzymes perform catalysis with high selectivity. We conclude with our personal viewpoint and hope that further developments in quantum chemistry and especially in the field of multireference wave function methods are needed to have a solid theoretical basis for the $NHFe_{(2)}$ studies, mostly by providing benchmarking and calibration of the computationally efficient and easy-to-use DFT methods.

Keywords Non-heme iron · Density functional theory · Multireference methods · Dioxygen activation · Reactivity

✉ Martin Srnec
srnec@jh-inst.cas.cz

✉ Lubomír Rulíšek
rulisek@uochb.cas.cz

[1] Institute of Organic Chemistry and Biochemistry, Academy of Sciences of the Czech Republic, Gilead Sciences & IOCB Research Center, Flemingovo náměstí 2, 166 10 Prague 6, Czech Republic

[2] J. Heyrovský Institute of Physical Chemistry, Academy of Sciences of the Czech Republic, Dolejškova 3, 182 23 Prague 8, Czech Republic

[3] Institute of Organic Chemistry, Research Centre for Natural Sciences, HAS, P.O.Box 286, Budapest 1519, Hungary

Introduction

Iron in any of its oxidation states is one of the most abundant transition metal ions in biological systems [1]. It can be mostly found in hemes, which not only store and transport O_2 but are also cofactors of many enzymes [2]. Besides hemes, one finds iron in the iron–sulfur clusters ([Fe–S] clusters), which are cofactors in numerous proteins with important redox, catalytic, or regulatory properties [3, 4]. Putting aside hemes and [Fe–S]-containing metalloenzymes, there remains a large family of non-heme iron enzymes (NHFe) [5]. Typically, these enzymes contain mono- or binuclear iron sites (NHFe and $NHFe_2$) with (O,N)-containing ligands and catalyze a broad set of oxidation reactions including H-atom abstraction for hydroxylation, halogenation, desaturation, peroxidation, ring closure of a substrate, electrophilic aromatic substitution for mono- or dioxygenation, or even phosphate-bond hydrolysis [5, 6]. It is not the purpose of this minireview to provide an exhaustive report on non-heme iron chemistry and spectroscopy, which can be found in extensive reviews (e.g., Ref. [5]). Neither do we attempt to give a full account of various reaction mechanisms of $NHFe_{(2)}$ enzymes studied by

quantum chemical methods, which have been also reviewed quite recently [7]. Instead, we want to highlight current challenges in the theoretical treatment of $NHFe_{(2)}$ sites in biological systems—mostly metalloproteins—and correlate the enzymatic activity with the catalytic properties of the small $NHFe_{(2)}$ synthetic models [8–10].

From a theoretical perspective, the $NHFe_{(2)}$ systems are considered one of the greatest challenges for contemporary computational chemistry. On top of the usual problems encountered in modeling of metalloproteins, such as the construction of an appropriate model (e.g., full protein vs. cluster representing the active site), selection of the methodology [e.g., molecular dynamics (MD) sampling, combined quantum mechanical and molecular mechanical (QM/MM) techniques, free-energy perturbation (FEP)], basis set considerations (large basis sets are required for many wave function techniques to obtain converged results), one may add the multitude of spin states available for the $NHFe_{(2)}$ systems [11, 12] including spin-state crossings and potentially large self-interaction errors when it comes to the description at the density functional theory (DFT) level [13].

At the same time, we are of the opinion that only concerted experimental and theoretical efforts [14] may lead to a deeper understanding of the fundamental question why nature selected iron as one of the most versatile transition metal ions to catalyze a broad spectrum of reactions (see above). Were iron-containing metalloproteins selected by evolution because they were the most efficient catalysts for the particular purposes? Or was it purely accidental, perhaps governed by the high abundance of iron in nature? What makes iron in its biological sites so special? Is it its intrinsic and remarkable electronic structure and the availability of the different spin states? Or does the variability of readily accessible oxidation states contribute to the reactivity? Or is the iron chemistry about the facile formation of the reactive intermediates, such as the Fe^{IV}=O compounds (which are at the same time a source of inspiration for the synthesis of small catalytic systems)? These and others are the open or semi-solved questions in $NHFe_{(2)}$ chemistry. We may not provide definite answers to these questions; this minireview rather aspires to provide inspiration for future studies in the field that may bring us closer to these long-sought answers.

There is one noticeable and slightly overlooked consequence of the often-emphasized "happy marriage" between theory and experiment in bioinorganic chemistry: the fact that many fundamental developments in modern quantum chemistry were driven by the complex electronic structure of transition metal-containing systems. Adjectives, such as highly open-shell, strongly correlated, entangled, spin-coupled, were in last decades both nightmares for quantum chemists as well as fuels for the development of new methods, techniques and approaches. Still, we feel that the absence of a robust and reliable ab initio wave function-based method that would enable calibration of popular DFT methods is the major obstacle and challenge in bioinorganic chemistry and even more so in the realm of $NHFe_{(2)}$ systems. Recent developments in this field represented by density matrix renormalization group (DMRG, vide infra) or various sophisticated constructions of the restricted active space multireference calculations (RASSCF/RASPT2) are quite promising, though these methods have not yet proven to be on par with what the single-reference coupled-cluster methods, such as CCSD(T), are in small-molecule closed-shell chemistry.

The organization of this paper is as follows: prior to embarking on a short tour through the recent methodological advances, we will shortly mention the importance of the correlation of spectroscopy and quantum/theoretical chemistry. The latter provides complementary information to experimental spectra, most notably the energy/structure mapping. The methodological overview will be then followed by selected examples in $NHFe_{(2)}$ chemistry where theory significantly contributed to unraveling new mechanisms and phenomena. These were selected to highlight the importance of computational studies in understanding $NHFe_{(2)}$ chemistry.

We may conclude the introductory paragraph by our personal experience from the studies of $NHFe_{(2)}$ systems, an experience most likely shared by others: correlation of calculated results with experimental—crystallographic, kinetic, electrochemical, spectroscopic—data resembles more than anything else a meticulous detective's work, at various stages frustrating and strenuous, but at the end often revealing and rewarding.

Quantum chemical methods in bioinorganic chemistry and in spectroscopy

Spectroscopy is a chemist's eye into the molecular world. This is especially true for the biological NHFe and $NHFe_2$ active sites and their synthetic mimics whose complex electronic structures result in remarkable spectroscopic properties, often manifested by well-defined spectral fingerprints. As such, experimental spectra provide a unique source of information on geometric and ground/excited state electronic structure properties. However, it is often, if not always, necessary to correlate the spectroscopic data with quantum chemical (QC) calculations. For many biological systems, it is also advantageous to carry out the QC/spectroscopic correlations for smaller crystallographically characterized synthetic models. Thus, the spectral features obtained on well-defined geometric structures of smaller models not only provide us with direct

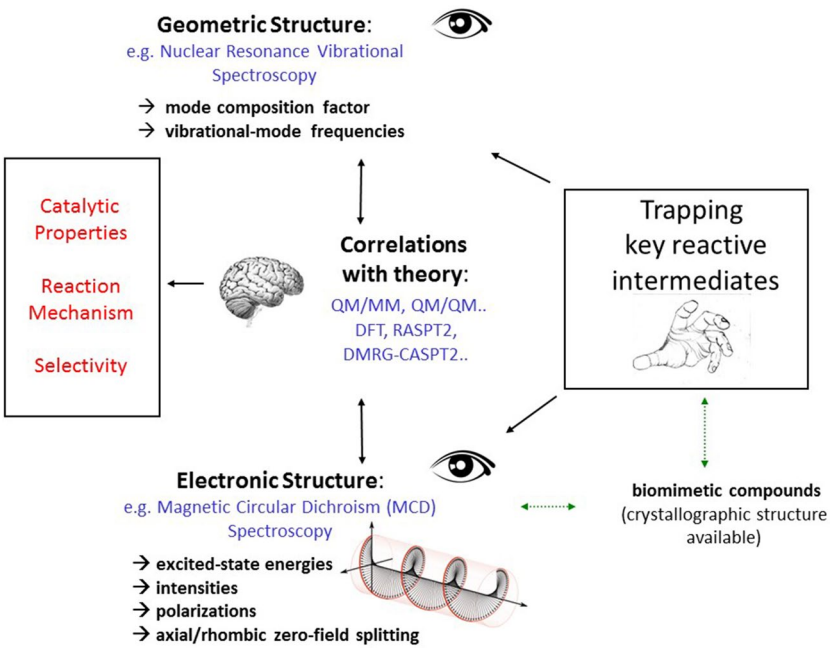

Fig. 1 The combined spectroscopic/theoretical approach for the investigation of geometric/electronic structures of enzymatic NHFe intermediates and their catalytic properties

experimental information of structural arrangements in complex sites in biological systems (e.g., metalloproteins), but it is also an excellent opportunity for calibration of electronic structure theory (Fig. 1). Such a calibration can be, for example, realized by selecting an appropriate QC method and basis set, incorporating/changing the amount of the Hartree–Fock electronic-exchange interactions in a DFT method, or determining the set of relevant orbitals for the complete or restricted active spaces in multireference wave function theories. The calibrated QC method can be then effectively employed for (i) understanding spectroscopic properties of similar (biological) NHFe active sites, which also allows to determine their geometric structures (if unknown otherwise), and (ii) providing an insight into their electronic structure properties (e.g., frontier molecular orbitals, spin density distributions, etc.) that can be directly correlated to reactivity and reaction mechanisms (Fig. 1). Calibration of the QC approaches against experimental spectroscopy complements benchmarking them against reliable "gold standard" quantum chemical methods, because these "reference" methods, in the context of bioinorganic chemistry, may be applicable only to strongly simplified models or may not exist at all. Still, such benchmarking and the accumulated general experience about the strengths and weaknesses of QC methods anyway form a basis for the choice of a particular method and for gaining confidence in its results. Indeed, in many successful computational studies, the small-model calibrations were the only guidelines. Nevertheless, calibration against spectroscopy can provide significant further support for the computational predictions and conclusions, or it can help choose the appropriate method where benchmarking and sufficient experience are either unavailable or inconclusive.

Density functional theory calculations of spectroscopic properties of $NHFe_{(2)}$ species

Due to the increase in computational power and efficiency of the algorithms, DFT and time-dependent DFT (TDDFT) methods can nowadays be routinely applied to predict various spectroscopic properties of model complexes or truncated enzyme active sites on the order of ~100 to 200 atoms or even more [15]. The treatable system size and the accuracy are often sufficient to reasonably link infrared (IR) and Raman, UV and visible absorption (UV/Vis Abs), circular dichroism (CD), electron paramagnetic resonance (EPR) and Mössbauer spectroscopic data to molecular geometries and to interpret the individual transitions in terms of the electronic structure, particularly if the exchange–correlation functionals are carefully chosen. Here, we present a selection of the cutting-edge problems that have been recently solved using a combination of DFT and spectroscopic techniques, grouped according to the roles played by the two methods. We also briefly mention the most interesting developments of methodology to make further branches of spectroscopy amenable to DFT/TDDFT treatment.

First, in spite of the wealth of information provided by the spectroscopic techniques themselves, DFT is often helpful to elucidate the nature of the observed spectral features. In a recent study of an Fe^{IV}-oxo complex of a tetramethylcyclam (TMC; 1,4,8,11-tetramethyl-1,4,8,11-tetraazacyclotetradecane; see Fig. 2) ligand with a pendant amide, formation of an unusual blue chromophore was observed upon

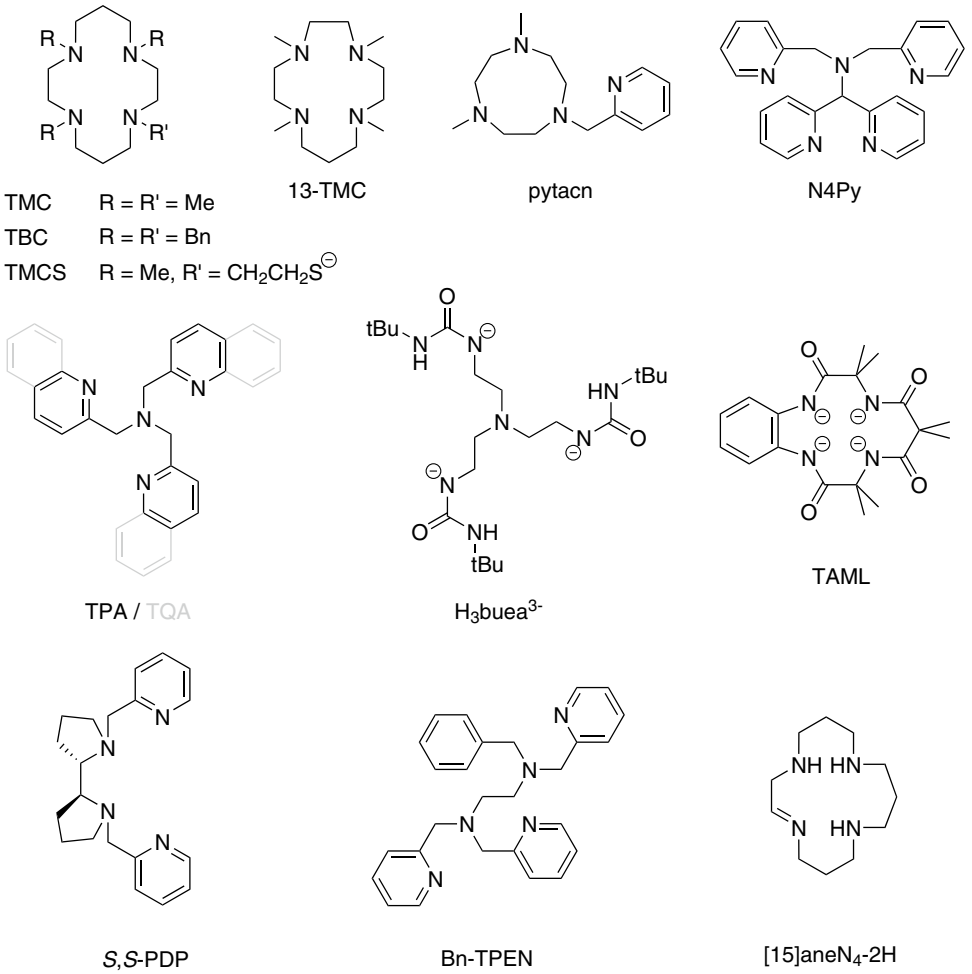

Fig. 2 Structures of some ligands employed in biomimetic non-heme iron complexes

deprotonation, which could be assigned using TDDFT to a ligand-to-metal charge transfer transition from the enolate-like amide donor to a vacant (Fe d + O p)* orbital [16]. TDDFT was also found to be helpful for understanding the observed changes in Fe/α-ketoglutarate (α-KG) π* metal-to-ligand charge transfer upon variations of H-bonding, and five- or sixfold coordination, which reflect stabilization of the α-KG π* orbital directly influencing O_2-reactivity in α-KG-dependent enzymes [17].

The degree of reliability of DFT/TDDFT allows the correlation of spectroscopic data with atomic level structures and makes it possible to choose from energetically comparable structural candidates. For example, with reference to computed Mössbauer data, a model of the TauD-***J*** enzyme intermediate could be assigned to $[Fe^{IV}(O)(TQA)(NCMe)]^{2+}$ instead of the five-coordinate and triflate-bound alternatives (TQA = tris(2-quinolylmethyl)amine; see Fig. 2) [18]. Similar correlations of Mössbauer data led to the suggestion of a protonated peroxo moiety in the peroxo intermediate of toluene/*o*-xylene monooxygenase hydroxylase (ToMOH) [19], while prediction of UV/Vis data allowed the identification of an unprotonated Fe^{II}–superoxo complex as the T1 intermediate in superoxide reductase [20]. Modeling of the UV/Vis, magnetic circular dichroism (MCD), and resonance Raman data established the binding mode of 4-hydroxyphenylpyruvate to the 3His-active site of the diketone cleaving dioxygenase Dke1 as the enolate [21]. Structures of intermediates in the $NHFe_2$ enzymes AurF [22], Δ^9 desaturase [23], methane monooxygenase (MMO) [24], and M ferritin [25] as well as in the NHFeMn enzyme class Ic ribonucleotide reductase (RNR) [26] and the relevant conformers of the ferrous soybean lipoxygenase [27] have also been established using this methodology. Prediction of Mössbauer spectral changes allowed to conclude the proton source in the radical transfer of a class Ia RNR to be the iron-bound water molecule [28].

On the other hand, correlation with spectroscopic data can be used to validate or actually choose ("calibrate") the DFT methodology for the description of electronic structure or reactivity. This approach was chosen in a comparative study of the high-spin/low-spin Fe^{III}–OOH O–O bond stretch, where confidence in B3LYP reaction coordinate calculations was gained from the successful reproduction of Abs and variable-temperature, variable-field

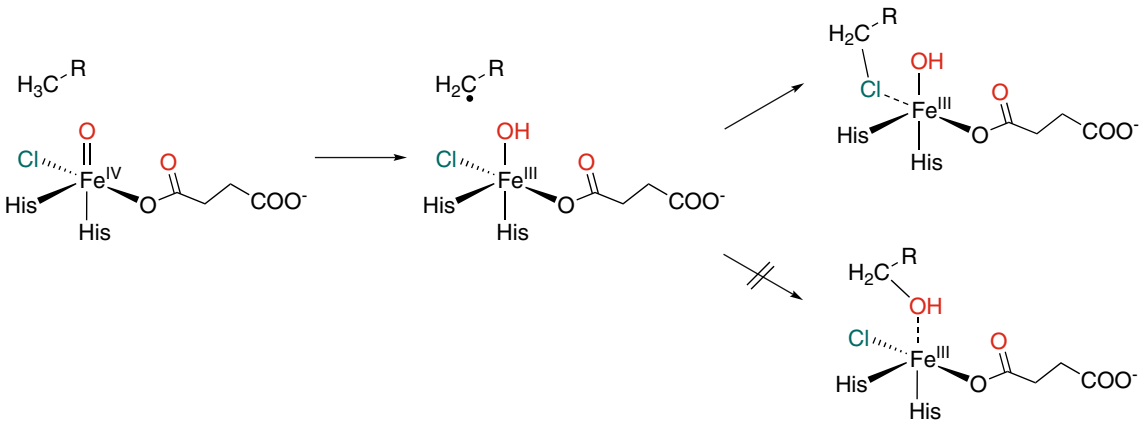

Fig. 3 Fe(IV)–oxo intermediate of the α-KG-dependent halogenase SyrB2 and its reaction with the substrate

(VTVH) MCD spectroscopic data [11]. In a study of nitrile hydratase, DFT was used both as a tool for spectral assignments and reaction coordinate calculations, with BP86 chosen because B3LYP overstabilized the high-spin states, and BP86 + 10 %HF did not reproduce good spectral differences between various forms of the active site [29]. At the same time, BP86 + 10 %HF was selected for the investigation of the O_2 reactivity of 4-hydroxyphenylpyruvate dioxygenase (4-HPPD) on the basis of calibration on NO complexes (a widely employed O_2 surrogate for spectroscopic purposes), with B3LYP underestimating the charge transfer from Fe to NO [30]. Interestingly, the success of spectral predictions showed B3LYP to be appropriate for describing the electronic structure of NO bound to cysteine dioxygenase model complexes [31]. Finally, for a functional model complex of iron superoxide dismutase, modeling of absorption and Raman spectra suggested the preference for X-ray crystallographic instead of DFT-optimized geometries [32]. In a more general sense, validation against experimental spectroscopic data has also been used to provide general benchmarks of computed Mössbauer data [33, 34].

Beyond the UV/Vis/near-IR electronic transitions, the IR/Raman-based vibrational spectra, and the EPR and Mössbauer data, theoretical developments have turned to new spectroscopic approaches. Recently, it has been shown that the ^{1}H NMR spectra of paramagnetic species, specifically, Fe^{IV}–oxo complexes, can be predicted to a reasonable accuracy, allowing correlation of NMR data to structures and spin states [35]. Promising advances in TDDFT or DFT/CI-based (CI, configuration interaction) approaches have been made towards the calculation of various X-ray absorption and emission features relevant for iron complexes [36–39], again with the potential of structural assignment or electronic structure calibration [40, 41]. Nuclear resonance vibrational spectroscopy (NRVS), selectively probing the iron-containing vibrational modes using nuclear excitations with synchrotron radiation, has lately become an important tool in the bioinorganic chemistry of iron systems. DFT methods usually perform well in predicting NRVS spectra, and the accumulation of reference data concerning spectral features of structurally well-characterized $NHFe_{(2)}$ model complexes has been initiated [42, 43]. NRVS spectroscopy in conjunction with DFT has already demonstrated its potential in the structural assignment of samples, as shown for the Fe^{IV}–oxo intermediate in the α-KG-dependent halogenase SyrB2 (see Fig. 3) [44], and for the Fe^{III}-bound and activated forms of the anticancer drug bleomycin [45]. NRVS with DFT has also proven useful in defining steric effects in NHFe model complexes [46]. As part of the development efforts, the necessary size of active site models has been explored for NRVS [47] and also for Mössbauer parameter modeling [48].

Correlated wave function theory calculations of spectroscopic properties of $NHFe_{(2)}$ species

Although most of the quantum chemical calculations on $NHFe_{(2)}$ species are carried out employing computationally highly efficient Kohn–Sham DFT (KS-DFT), this methodology might not be always well suited for these and many other systems of bioinorganic interest. Electronic structure of open-shell NHFe systems, and especially of the magnetically coupled binuclear $NHFe_2$ sites may possess strongly multiconfigurational character even in—otherwise less problematic—high-spin states. Their electronic structure may not be correctly described with currently available DFT functionals. In addition, most of spectroscopic properties require calculation of not only the ground, but also excited electronic states. Therefore, it is highly desirable to be able to perform computationally more demanding calculations based on correlated wave function methods. These methods can be, depending on the reference wave function,

divided into two main classes—single-reference (SR) and multireference (MR).

As was shown by Taylor already in early 90s [49], the computationally most affordable SR method—Møller-Plesset second-order perturbation theory (MP2)—tends to produce fairly poor results for transition metal compounds, and one thus should use rather higher level methods. Among these, coupled-cluster with single and double (and perturbative triple) excitations—CCSD(T)—is usually the method of choice. The canonical CCSD(T) method with formal the scaling of $\sim O(N^7)$, or more precisely $\sim O(O^3V^4)$, where N is some appropriate measure of the size of the system and O, V are the number of occupied and virtual orbitals, respectively, is quite expensive and this fact limits its application to small model complexes (we consider 30–40 atoms as a practical limit). However, significant progress has been made in the development of "linear-scaling" approximations based on local correlation, see, e.g., Refs. [50–52]. The approximate coupled-cluster methods are presently applicable to systems containing several tens of atoms, which is the size of many metalloenzyme active site cluster models. For example, Dieterich et al. have reported calculations for the molybdenum active site of aldehyde oxidoreductase [53], while Neese and co-workers carried out coupled-cluster calculations for the carbonmonoxyheme center [54]. Although the development and increasing range of applicability of SR coupled-cluster methods for theoretical studies in bioinorganic chemistry are highly promising, there remains a problem in the reliance on a single-reference wave function and treatment of static correlation. Sometimes, it can be circumvented by performing calculations with broken-symmetry reference, or using completely renormalized CCSD(T) [CR-CCSD(T)] [55], which has been successfully applied to the theoretically challenging problem of Cu_2O_2 core isomerization [56]. However, the inadequacy of using a single determinant for the reference wave function is the main reason for the prevalence of MR ab initio methods in the realm of $NHFe_{(2)}$ systems—one of the most difficult species in this respect.

The multireference treatment is usually based on the complete active space self-consistent field (CASSCF) reference wave function, which is constructed as a linear combination of all possible configurations with particular spin and spatial symmetry arising from distribution of N electrons in M orbitals, referred to as CASSCF(N,M). This method has already proven useful for a large variety of chemical problems, including applications in bioinorganic chemistry. Just to mention a few studies—Roos et al. have conclusively assigned the oxidation state of iron in chloroiron corrole [57], and Chen et al. and Nemukhin et al. studied Fe-O_2 bonding in heme and non-heme active sites by combined QM(CASSCF)/MM methodology [58, 59]. Although CASSCF brings in highly valuable insight into the electronic structure of complex systems, and it is an exact method in the sense that it converges to the full-CI solution upon enlargement of the active space, it has two problems which should be stressed here. The first problem is that its exponential scaling severely limits the size of active space used in practice. Taking into account the usual C_1 symmetry of metalloenzymatic active sites, calculations with active spaces larger than approximately 15 electrons in 15 orbitals are prohibitively expensive, and this practical limit has been around for a decade. This limitation becomes especially important for systems with multiple metal centers like $NHFe_2$. Secondly, CASSCF is far from being a "black box" method, and proper choice of the active orbitals requires substantial experience and experimentation. In a conventional manner, the former can be often avoided by use of approximate approaches, such as restricted/generalized active space SCF (RASSCF/GASSCF) methods, where limited excitation levels from/to various active-orbital subspaces are used [60–62].

An interesting alternative to these methods emerged in the recent development of density matrix renormalization group (DMRG) theory, first proposed for quantum chemistry by White [63], and thoroughly reviewed by various groups since then [64–68]. The reduced polynomial scaling of DMRG-CASSCF with respect to the size of active space enables the inclusion of up to approximately 40 active orbitals in general, or even 100 orbitals in special cases, which is already sufficient for many applications concerning multi-center active sites. Recent calculations of the electronic structure of Mn_4CaO_5 cluster of photosystem II [69] and low-energy spectra of iron–sulfur clusters [70] can serve as a demonstration of its capabilities. However, because the DMRG wave function is only an approximation to the active space full-CI solution, its quality may quite strongly depend on the shape and ordering of active orbitals. For a typical calculation concerning a metalloenzymatic active site, carefully ordered localized active MOs are usually the best choice according to our experience. The selection of appropriate active space is a non-trivial task for any active space-based calculation, and only very recently Stein and Reiher reported an attempt to develop an automated method for active space selection using DMRG entanglement analysis [71]. It remains to be seen whether this procedure can substitute human intuition and chemical experience in selecting an appropriate active space.

Due to the limitations of the active space size, which for the molecules typically studied, contains only a fraction of the valence-shell orbitals and electrons, thus leaving the rest of them uncorrelated, active space-based calculations are nowadays often complemented by associated methods for treatment of dynamic correlation. Similar to the SR case, the most accurate methods "available" are

based on multireference coupled-cluster (MRCC) theory. In its explicit form, MRCC theory is highly complex and has been applicable only to small molecules so far. However, when a fully internally contracted scheme is used, as in the case of canonical transformation (CT) theory [72], dramatic reduction of the complexity is achieved and, therefore, the method can be of interest for bioinorganic chemistry in the near future. For example, DMRG-CT with large active space has been already applied to the model complexes with a Cu_2O_2 core [73, 74]. Similar limitations, although less strict, apply also to the multireference configuration interaction (MRCI), unless it employs either full internal contraction [75] (see Ref. [76] for a recent study on the splitting of low-lying states in iron–oxo porphyrins), or a posteriori selection of configurations [77, 78]. Thus, most of the present MR calculations rely on the second-order perturbation theory (PT2) methods, such as complete/restricted active space PT2 (CASPT2/RASPT2), or *N*-electron valence space PT2 (NEVPT2), which overcome some of the peculiarities of the former approaches. Although these methods are fairly efficient and can be used for relatively large systems, the lower level treatment of dynamic correlation by perturbation theory brings in some difficulties—usually illustrated on the correlation of transition metal valence *d* orbitals, which may require inclusion of higher shell *d* orbitals into the active space to obtain realistic results (the so-called "double-shell" effect—see, for example, Ref. [79]). In addition to general problems related to the CAS treatment (see above), when using RASPT2 or CASPT2 methods one has to deal with yet another technical issue, the so-called IPEA (ionization potential-electron affinity) shift. The concept of IPEA shift was put forward by Roos and co-workers to correct systematic errors due to the imbalanced treatment of closed and open shells, and a value of 0.25 au was suggested semi-empirically [80]. Recently, however, several authors have shown that the spin state energies depend drastically on the value chosen for it. Some have argued for a value of 0.50, while others have proposed a value of 2.0 [12]. The PT2-based approaches with conventional reference wave functions have been applied to both NHFe and $NHFe_2$ representative active sites or geometrically related model complexes [81–84]. Recently, a DMRG-CASPT2 study for the active site of $NHFe_2$ Δ^9 desaturase (Δ^9D) was reported, showing that this state-of-the-art methodology can be used also for metalloenzymatic reactivity [85]. In this study, it has been shown that a set of respectable DFT functionals provide quite varying activation energies for the first hydrogen abstraction step in the desaturation reaction and cannot provide an unambiguous answer as to whether hydrogen is abstracted as a hydrogen radical or a hydride anion.

Although MR methods can treat not only dynamic, but also static correlation, one should be aware that this is done with limited accuracy, especially for larger complex species like metalloenzyme active sites. These methods have also some other advantages over DFT and SR methods used for calculation of spectroscopic properties. Many of these, such as spin–spin *J* coupling constants or absorption spectra, can be accessed by MR calculations directly, without the need for any additional computational effort. Others, which involve spin–orbit coupling, Zeeman and other effects, can be calculated either by means of linear-response theory, common to DFT and SR correlated methods, or by means of quasi-degenerate perturbation theory (QDPT), also referred to as state interaction (SI) method in this particular case. Spectroscopic properties like, for example, electronic paramagnetic resonance (EPR) *g*- and *A*-tensors, MCD spectra, zero-field splitting (ZFS), are nowadays becoming accessible in available quantum chemical codes.

In summary, we believe that recent developments in the field of correlated ab initio methods are highly encouraging, and these methods are expected to be of an increasing interest in the near future, not only to theoretical bioinorganic chemists.

Theoretical tools for the description and analysis of electronic structure

Electronic states of various spin quantum numbers are, in transition metal compounds, often "near-degenerate", as a consequence of the small energetic splitting of the transition metal *d* orbitals. This is especially true if multiple metal centers are present. Then, the spin multiplicity of the ground electronic state can vary depending on the chemical surroundings of the metal ions. Moreover, metal *d* orbitals may act as electron donating as well as electron accepting orbitals. Thus, multiple reaction pathways, involving various spin states, are in principle possible, and the origin of the measured spectroscopic parameters may be uncertain as well. Given these difficulties, theory can provide highly valuable information, supplementing the initial understanding obtained by experiments. Detailed analysis of the calculated wave functions may answer key questions regarding, for instance, the oxidation states of the metal centers and surrounding atoms, the changes in electronic structure during reactions, the character of spectral transitions, etc. In this section, we will briefly discuss the main aspects of electronic structure analysis and some of the tools introduced recently.

Owing to the fact that quantum chemical methods almost exclusively rely on the MO-LCAO ansatz (molecular orbitals as linear combinations of atomic orbitals), the key ingredient of any electronic structure analysis is the characterization of the composition of occupied MOs. The MO occupation numbers are usually restricted to integers (e.g., in DFT and HF calculations), but they can be defined

by real numbers as well, reflecting the electron correlation accounted for by SR and MR methods. This analysis involves the assignment of the AOs with dominant contributions to the particular MO which also reveals information about the MO type (e.g., σ, π, etc.). By doing so, the theoretical results calculated at any level of theory can be to some extent "mapped" onto the traditional molecular-orbital diagrams. Such mapping has been found to be useful and important for the qualitative understanding of the nature of the bonding in transition and other metal systems. For example, the oxidation state of a metal center can be deduced from the number of electrons in MOs with predominantly metal *d* character, and its possible spin states from the number of corresponding singly occupied orbitals. It must be emphasized, though, that such assignments may become difficult and ambiguous for multiple reasons—formation of covalent metal–ligand bonds, strong delocalization of MOs, use of an unrestricted scheme, etc. Thus, various tools that help to overcome some of these difficulties have been developed.

Most of the calculations for open-shell transition metal systems are carried out within the unrestricted KS-DFT (UKS) framework. UKS gives rise to two separate sets of MOs: for α and β electrons. Provided that the spin contamination is small, it is useful to analyze the so-called quasi-restricted orbitals (QROs), which can be derived from unrestricted natural orbitals [86]. Using QROs, one recovers the more familiar picture of one set of doubly or singly occupied and empty MOs. In case of low-spin electronic states, broken-symmetry DFT solutions are often used, which imply significant spin contamination. For this kind of wave function, unrestricted orbitals reordered by the corresponding orbital transformation (COT) can be, based on the spatial overlap for α and β pairs, classified as doubly occupied, spin coupled ("magnetic" pairs of singly occupied orbitals—one carrying α, other β electron) or unpaired (singly occupied by α electron or empty) [87]. Importantly, analysis of the unrestricted corresponding orbitals (UCOs) obtained by COT may also give some insight into the strength and pathway of antiferromagnetic coupling if multiple metal centers are present. Other useful information about the singly occupied orbitals of a molecule may be gained from spin-natural orbital (SNO) analysis.

It can be mentioned that also traditional tools and concepts, such as Mulliken population analysis and frontier molecular orbitals (FMOs), bring in highly valuable insight into the electronic structure of molecules. In the framework of single-determinantal methods, the latter has proven to be one of the most powerful concepts for understanding chemical reactions, providing a link between electronic structure and chemical reactivity, which are intimately coupled, as well as for the interpretation of experimental electron affinities and ionization potentials. The reaction mechanisms are typically described by the changes in the FMOs' character during the reaction, and the FMOs' energetic splitting is correlated with the activation barrier. Moreover, the ability of a molecule to undergo a certain type of reaction may be in many cases judged by examining the electronic structure (FMOs) of only the reactants [88]. The study of Srnec et al. [81] may serve as an example of FMO analysis for an NHFe model complex.

For conventional MR correlated wave functions, MO analysis is supplemented by the analysis of the so-called CI (configuration interaction) vector, which bears information about the contributions of particular configurations to the wave function. For a typical calculation on a transition metal complex, the CI vector obtained at the CASSCF level—often expressed in localized active MOs, which simplifies, for example, metal *d* configuration assignment—is analyzed. Although the electronic character of the studied states is defined already by the natural orbitals (NOs) and their occupation numbers (NOONs), which are often used for basic characterization, examining the CI vector, i.e., analyzing the nature of dominant electronic configurations and their weights in the total wave function, provides significantly more detailed information. The mechanisms of chemical reactions can be depicted in a way analogous to FMO analysis, following the changes in the active-orbital composition and CI coefficients. However, MR calculations provide also information about the changes in static correlation effects (degree of multiconfigurational character) during the reaction, which may be, to some extent, used as a measure of the possible breakdown of DFT and SR methods for some, usually transition state, geometries. Regarding the importance of CI vector analysis, DMRG represents a somewhat special category of multiconfigurational methods, because the CI coefficients are generally not accessible by DMRG calculations. However, alternative tools, such as the analysis of orbital entanglement (mutual information) and one-orbital entropy, have been introduced to the DMRG framework. These can provide a similar type of information to that available from the CI vector analysis (see, for example, Refs. [69, 70] for their applications to the electronic structure analysis of complex transition metal compounds).

$NHFe_{(2)}$ reactivity: correlating theoretical calculations with thermodynamic and kinetic experimental data

Besides correlating the QC calculations with spectroscopy—which is in fact also the structure/energy mapping—theoretical data also provide a unique opportunity to relate the overall thermodynamics and kinetics of the catalyzed

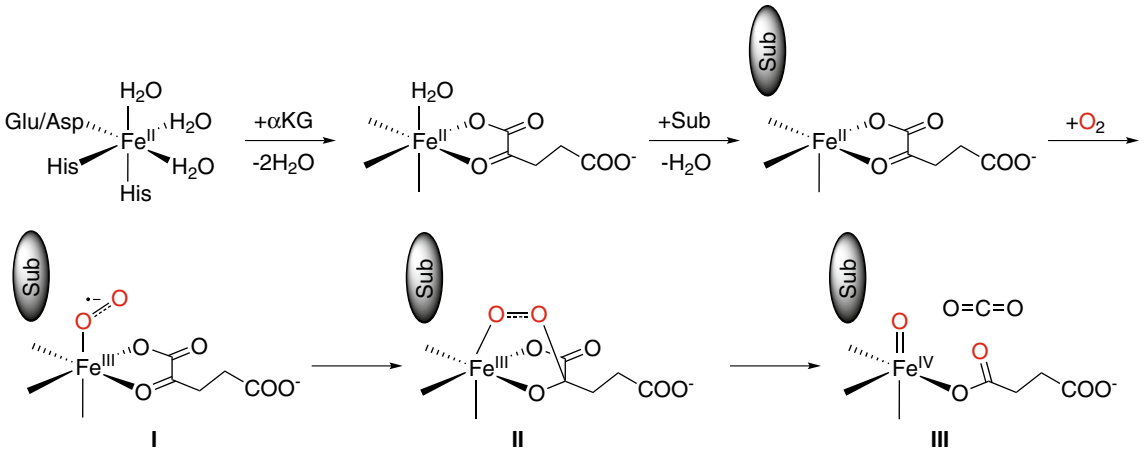

Fig. 4 Consensus mechanism of the oxygen activation in α-KG-dependent enzymes

reactions with the mechanistic view of individual chemical transformations occurring in the studied catalytic cycle. In the following, we will mostly focus on reaction coordinates as descriptors that greatly assist in elucidation of various steps in reaction mechanisms of $NHFe_{(2)}$ compounds. By calculating reaction barriers (activation energies) for plausible pathways, one can distinguish elementary steps in the overall process (O_2 activation, hydrogen atom abstraction, etc.). Ideally, the calculated activation energies have to match the experimental rate constants and unravel or confirm the rate-determining step (RDS) whereas the primary and secondary H/D kinetic isotope effects observed experimentally provide further information on whether and how a transfer of hydrogen is involved in the RDS. Nevertheless, inaccuracies in the computed activation energies often preclude the unambiguous assignment of the reaction mechanism or unique reaction coordinate and rather allow for separation of a set of several "competing" pathways from other ones. In redox-active $NHFe_{(2)}$ chemistry, the overall thermodynamics is also controlled by the electron accepting or donating properties of the reactive intermediates involved. This is quantified by the reduction potentials (amenable to fairly accurate computations) [89]. Last but not least, most of the $NHFe_{(2)}$ catalyzed reactions involve proton transfer(s) that are controlled by the acidity constants of the species involved, presumably fine-tuned to support the proton transfer at the specific step of the overall reaction. These and related issues will be the subject of the following chapters.

Modeling O_2 and H_2O_2 activation pathways

To be usefully reactive toward the singlet closed-shell organic substrates, triplet O_2 must be activated by converting it to a reactive species, some kind of iron–oxygen intermediate in the case of $NHFe_{(2)}$. Many common themes are known by now, but the diversity of the enzymes and the complexity of the processes (including controlled oxygen access to the active site and substrate binding order, the nature of the reactive intermediates, and the factors that poise them toward specific reaction channels) still provide us with new conundrums. In this section, the most recent contributions to this area are overviewed to highlight the pertinent challenges in theoretical modeling. Studies on the related H_2O_2 activation processes by bioinspired non-heme iron complexes are also touched upon briefly.

α-KG-dependent enzymes

A wide family of NHFe enzymes carry out $2e^-$ oxidation of their substrate while the remaining $2e^-$ required for O_2 reduction come from the oxidation of their co-substrate, α-ketoglutarate (α-KG) to succinate and CO_2. It has been proven that co-substrate oxidation happens first, ultimately producing a reactive Fe^{IV}=O species utilized in subsequent chemistry (Fig. 4). Following co-substrate and substrate coordination, the initiating step of the actual chemistry is the binding of O_2 to the Fe^{II}-α-KG complex to yield presumably Fe^{III}–superoxo (**I**). As a prerequisite, the last H_2O ligand of iron dissociates upon binding of all the organic substrates, and computations were carried out to identify factors promoting the dissociation. Substrate steric effects, H-bonding with the second-sphere residues, and the electron-donating character of α-KG were found to cooperate in the well-timed expulsion of H_2O, which contributes to the selectivity of the catalysis by avoiding the unwanted generation of high-valent oxygen species [90]. The actual binding of O_2 is also influenced by many factors. In a study of the JMJD2A histone demethylase, carrying out energy decomposition on the basis of MD + QM/MM data, the favorability of this step was shown to be sensitively dependent on the extended protein environment [91]. Small

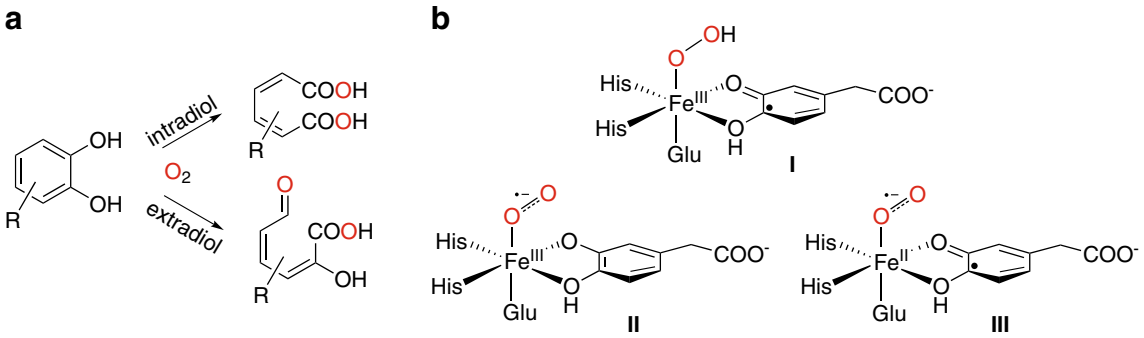

Fig. 5 **a** Reactions catalyzed by intradiol- and extradiol-cleaving catechol dioxygenases. **b** Some possible structures of the active species in 2,3-HPCD. Note that in the semiquinone forms (**I** and **III**), the delocalization of the organic radical is not depicted

models may thus not be capable of explaining the effects of mutants and inhibitors on O_2 binding. The role of the canonical (2His-1Asp/Glu) and alternative (3His) facial triads in determining the fate of the ketoacid co-substrate has also been addressed, and it was concluded that the 3His triad induces a different binding mode of the substrate (as dianion instead of monoanion), which triggers different reactivity (C2–C3 instead of C1–C2 cleavage) [21]. Furthermore, additional mechanistic complexity may arise in certain cases from a flexible α-KG binding, leading to multiple coordination sites for the incoming O_2 or multiple isomers of the resulting Fe^{IV}=O, which may contribute to enhancing the selectivity toward the desired iron oxidant for substrate conversion [44, 92, 93].

Besides all the above issues, the mechanism of the conversion of Fe^{II} + O_2 to Fe^{IV}=O seems also not to be settled yet, because the electronic structure, and even the existence, of some intermediates are very sensitive to the DFT functional used. A study using B3LYP predicted the first O_2 adduct to be an end-on Fe-dioxygen species (as **I** in Fig. 4), with the $S = 1,2,3$ states lying close in energy and exhibiting various contributions from Fe^{II}-dioxygen and Fe^{III}–superoxo resonance structures [94]. The bicyclic intermediate (**II**), formed upon the subsequent attack of the distal O on the α-keto group of α-KG, is a TS rather than local minimum on the favored quintet and septet PESs, and the associated reaction also involves C–C cleavage. On the triplet surface, **II** is a high-lying minimum. In contrast, BP86 + 10 %HF calculations indicated that the first step of O_2 activation is appreciably more favored on the triplet PES and directly yields an Fe^{IV}-peroxo bicylic intermediate (similar to **II** on Fig. 4 with Fe^{IV} instead of Fe^{III}), which further undergoes the decarboxylation process through $S = 1 \rightarrow S = 2$ crossover leading to the $S = 2$ Fe^{IV}=O product. The $S = 2$ and $S = 3$ O_2 adducts have end-on structures (**I**) and lie higher in energy [30]. BP86 + 10 %HF was chosen because it provided good description of spectroscopic properties of NO adducts and correctly predicted the amount of charge transfer from Fe to NO [94]. B3LYP underestimated the latter; yielding structures too close to Fe^{II}–NO• instead of Fe^{III}–NO^-, and it was argued that the same underestimation is the reason why formation of the Fe^{IV}–peroxo was not favored [94]. On the other hand, B3LYP was supported by CCSD(T) and NEVPT2 benchmarks on small models of the proposed intermediates [30]; nevertheless, the benchmarks were carried out with B3LYP geometries, and they did not include the triplet bicyclic structure. As neither approach for validating the employed functionals refers directly to the involved O_2 adducts, the question remains open until more accurate computations are available.

Ring-cleaving dioxygenases

Ring-cleaving dioxygenases catalyze the $4e^-$ oxidation of hydroxylated aromatic rings into open-chain aldehyde/carboxylic acid products using O_2. Classic examples involve catechol dioxygenases cleaving a 1,2-dihydroxylated ring in 1,2 (intradiol) or 2,3 (extradiol) positions (Fig. 5, part A). Challenges in modeling the O_2 activation stem from the fact that besides the variations in the iron–O_2 system, the substrate itself may also be $1e^-$ oxidized to a semiquinone (SQ) form, and the enzyme environment is crucial in tuning the relative stabilities of the various partially oxidized/reduced structures. In this respect, in the extensively studied Fe^{II}-containing extradiol homoprotocatechuate 2,3-dioxygenase (2,3-HPCD), experiments with the H200C mutant led to the characterization of an SQ•-Fe^{III}–hydroperoxo species, formed by PCET from Fe^{III}–superoxo and shown by the computations to be catalytically competent (Fig. 5, part B, species **I**) [95]. At the same time, Fe^{III}–superoxo (**II**) and hybrid Fe^{III}–superoxo/SQ•-Fe^{II}–superoxo (hybrid **II/III**) species were claimed to be active in wild-type 2,3-HPCD with 4-nitrocatechol [96] and with the native substrate [97], respectively, pointing to a difference in electron donating capability between the two substrates.

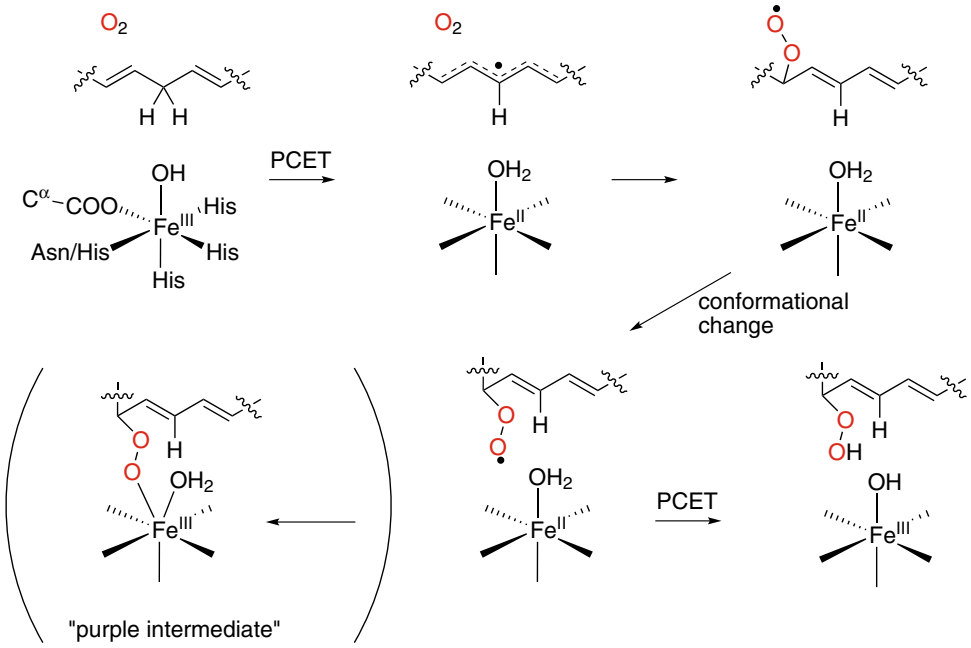

Fig. 6 Key steps of the lipoxygenase reaction mechanism

However, the hybrid species was not reported in an earlier study using a cluster model of the enzyme active site, highlighting the essential contributions of the environment in stabilizing SQ•-Fe^{II} structures [98]. Moreover, the different enzymatic environment provided by 3-hydroxyanthranilate 3,4-dioxygenase [99] seems not to stabilize the hybrid species either. Structures along the energy profile of 2,3-HPCD have also been the subject of research, and computational studies proved invaluable in cross-checking conclusions from indirect experimental evidence, including the question of homolytic/heterolytic cleavage of the O–O bond in the peroxo intermediate [100] and the nature of the crystallographically observed *gem*-diol structure [101].

Theoretical studies of O_2 activation have also been done recently on other related systems. For salicylate dioxygenase [102], a hybrid of Fe^{II}–O_2 and "SQ•"-Fe^{II}–superoxo electronic structures was found to prevail, with Fe^{II} playing a key role in mediating the synergism between substrate and O_2 activation. Using models of intradiol dioxygenase enzymes, several aspects of intradiol cleavage were addressed, including partial dissociation of the substrate to allow O_2 activation on the metal [103], stereoelectronic reasons for intradiol selectivity [104], and the possible noninnocence of the coordinating tyrosine ligand [105].

Miscellaneous monoiron systems

The O_2 activation reactivity at certain NHFe centers may be less amenable to classification into some of the big families. The involved diverse chemistries can provide important additional information about the possible tuning of O_2 activation. For example, theory revealed the roles of the iron oxidation state [106], the spin state and solvent exposure [107], the axial cysteine ligand [108], and the H bonds toward this ligand [109] in controlling the Fe–O vs. O–O bond breakage and the protonation of the Fe–O–O complex in superoxide reductase, as well as information about the overall mechanism [110]. Studies on cysteine dioxygenase [111] and on its model complex [112] clarified the full O_2 activation mechanism; clues as to the role of the thiolate ligand [113] and to the differences in pertinent O_2 activation pathways explaining why the enzyme cannot oxidize selenocysteine were also obtained [114, 115]. O_2 activation [116, 117] and the preceding required water dissociation [118] was also investigated in the tetrahydrobiopterin–iron amino acid hydroxylases.

The detailed inclusion of environmental effects is often required to achieve realistic conclusions about O_2 reactivity. For example, in hydroxyethylphosphonate dioxygenase (HEPD), water molecules trapped in the active site were identified to directly participate in the catalytic process [119], highlighting an aspect that was overlooked in the earlier QM-only study [120]. In lipoxygenase, computations on a QM-only model suggested exothermic formation, hence, possible catalytic relevance, for a seven-coordinate intermediate with the substrate peroxyl bound to the iron center (referred to as the purple intermediate; see Fig. 6) [121]. Detailed protein modeling showed that this intermediate is significantly destabilized, and its formation cannot compete with direct proton-coupled electron transfer from iron-bound H_2O to the peroxyl radical [122]. Protein dynamics, typically neglected in computational studies, were found to influence the energetics of the O–O cleavage step by several kcal mol in isopenicillin-N-synthase

(IPNS), highlighting also the potential of such effects in the further fine-tuning of reactivity [123].

The above studies illustrate that as more and more simplifications are used to treat a protein system, the probability of getting qualitatively wrong conclusions increases. The effect of simplifications in our computational models cannot be assessed within the model itself. One can gain confidence in the conclusions from a computational model when a large amount of experimental data is available and it can all be explained, when there are higher level studies of closely related systems indicating the validity of the approximations, and when chemical intuition suggests a high level of error cancelation for the investigated steps. In this respect, it is interesting to mention the QM-cluster study on the chemistry of hydroxypropylphosphonic acid epoxidase (HppE), where favorable binding of O_2 to the iron center and reasonable barriers for substrate oxidation were obtained using DFT [124]. However, it transpired from later experiments that the enzyme is inactive with O_2; it hardly even binds it, and it actually employs H_2O_2 as oxidant [125]. Answering why the QM-cluster calculations failed to detect the flaw in the assumptions would need a separate, higher level study, but one can expect that the effects of the neglected or approximated environment may be quite significant for the step when O_2 is transferred from aqueous solution through the protein cavities to the iron within the active site pocket, and may be less so for the inner sphere chemistry occurring thereafter. Indeed, the suggested substrate oxidation pathway starting from a Fe^{II}–hydroperoxo structure (which was a proposed intermediate of O_2 activation) remains consistent with the new experimental observations.

Diiron systems

$NHFe_2$ systems present further challenges for modeling due to the immense variety of possible isomers and the complicated electronic structure with a typical antiferromagnetic coupling between their high-spin iron centers. Selective formation of one or the other oxidant may be the result of precise tuning, the understanding of which requires a multilevel approach. This was demonstrated in a study comparing O_2 activation in methane and toluene monooxygenases, where the crucial role of the conformation of a second-shell threonine was identified [19]. Detailed studies including energy decomposition were also done on *myo*-inositol oxygenase (MIOX) to characterize the contributions to O_2 binding [126]. A comparison of O_2 cleavage using MnMn, MnFe, and FeFe active sites in ribonucleotide reductases allowed to explain the choice for the MnFe version in the absence of the radical-bearing tyrosine [127]. In spite of these successes, the diiron centers may sometimes present unsurmountable challenges for DFT. As mentioned above, we have recently undertaken a study on O–O bond cleavage and various other mechanistic aspects in Δ^9D using large-scale multireference ab initio calculations and found that none of the tested DFT functionals could adequately predict the preferences toward various pathways [85].

Model systems

Besides modeling the enzymatic systems, calculations proved useful in enhancing our understanding of bioinspired NHFe complexes. They contributed to the consistent mechanistic picture of the carboxylate-assisted NHFe/H_2O_2 epoxidation of organic substrates using PDP (2-({(*S*)-2-[(*S*)-1-(pyridin-2-ylmethyl)pyrrolidin-2-yl]pyrrolidin-1-yl}methyl)pyridine) or TPA (tris(2-pyridylmethyl) amine) ligands (see Fig. 2 for structures), clarifying the role of ferric peracetate and perferryl acetate complexes [128, 129]. A related system [Fe(pytacn)] for C–H oxidation without carboxylic acids was also studied successfully (pytacn = 1-(2-pyridylmethyl)-4,7-dimethyl-1,4,7-triazacyclononane; see Fig. 2) [130]. Analysis of sulfoxidation by $[Fe(TMC)OOH]^{2+}$ provided useful qualitative rules for homolytic or heterolytic O–O cleavage depending on *d* orbital occupations [131]. The power of computations was elegantly demonstrated in an exhaustive DFT and CCSD(T) study of the possible isomers and spin states of the ferric superoxo complex $[Fe(TMC)(O_2)]^{2+}$, corroborating previous experimental data [132].

As the most simplified "model" system of high-valent iron–oxo chemistry, the Fenton reaction, i.e., that of aqueous $Fe^{2+} + H_2O_2$, was also considered from a theoretical perspective. It turned out that various DFT functionals give different energetics for the possible pathways; however, when selected on the basis of high-level benchmark computations, it was possible to arrive at conclusions in accordance with experimental data [133]. H_2O_2 activation leading to Fe^{IV}=O was also successfully modeled for $Fe(TMC)^{2+}$ in the presence of an added base [134].

Modeling H-atom abstraction pathways

One of the most prominent reactivity features of mono- and binuclear non-heme iron species is their capability of homolytic cleavage of strong aliphatic C–H as well as O–H/N–H bonds (=H-atom abstraction abbreviated as HAA) that initiates various chemical transformations such as substrate hydroxylation, desaturation, halogenation, etc., making $NHFe_{(2)}$ (bio)chemistry incredibly rich and powerful (Fig. 7). From this perspective, it is not surprising that there has been an enormous experimental and computational effort in understanding the HAA reactivity of NHFe and $NHFe_2$ complexes and its effect on reaction (enzymatic) selectivity [135]. Selected theoretical contributions

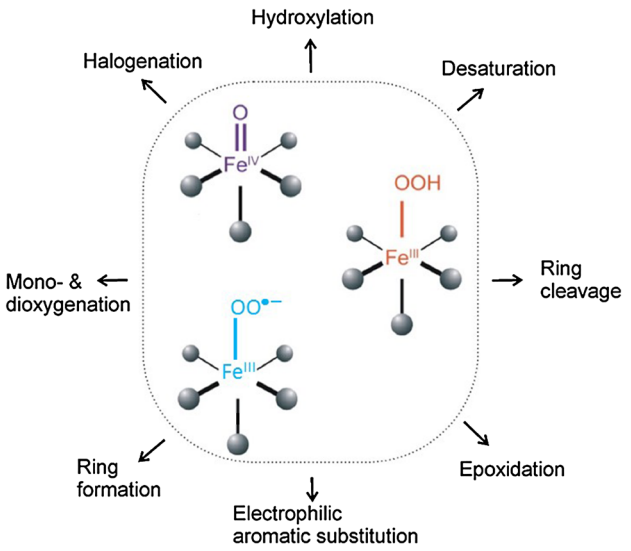

Fig. 7 The reactive NHFe species are competent for a wide range of substrate chemical transformations

advancing the knowledge in the field are briefly discussed below.

Mononuclear ferryl active site:
$C\text{–}H + O{=}Fe^{IV} \rightarrow C^{\bullet} + HO\text{–}Fe^{III}$

Theoretical studies in combination with spectroscopy, kinetics and product analyses were applied to various mononuclear synthetic and biological NHFe^{IV}=O active sites (e.g., in α-ketoglutarate or pterin-dependent NHFe enzymes) that allowed detailed understanding of electronic properties of Fe^{IV}=O and their contribution to HAA reactivity [6, 136–140].

It was demonstrated that three different mechanisms exist for HAA, depending on the spin state of the complex ($S = 1$ vs. $S = 2$) [81, 141, 142]. The triplet state, as the ground spin state of many synthetic NHFe^{IV}=O compounds, effectively operates only through a "π channel" with the C–H bond ideally oriented perpendicular to the Fe–oxo axis which allows the overlap of the substrate $\sigma_{C\text{–}H}$ orbital with one of the Fe=O $d\pi^*$ FMOs [141]. In contrast, the quintet state, which is the ground spin state in enzymatic NHFe^{IV}=O structures [143], has three HAA channels available: one "σ channel" that requires the C–H bond oriented in line with the FeO moiety ($d\sigma^*$ FMO overlapping with $\sigma_{C\text{–}H}$) and two "π channels" that both involve a $d\pi^*$ FMO but differ in the spin distribution of the Fe^{III} center ($S_{Fe} = 5/2$ vs. $S_{Fe} = 3/2$) [81, 140]. This HAA reactive channel flexibility hinted the importance of the $S = 2$ state for enzymatic selectivity [144]. Recently, low-temperature MCD spectroscopy in combination with CASPT2 and DFT calculations was used to define electronic structure of the NRVS-determined $S = 2$ Fe^{IV}=O active site in the halogenase SyrB2 and its contributions to H-atom abstraction, which was shown to proceed via the $\pi(S_{Fe} = 5/2)$ channel and to favor halogenation over hydroxylation [145].

It was also shown that $S = 1$ NHFe^{IV}=O species may be as reactive as the $S = 2$ systems, i.e., the HAA barrier associated with the $S = 1$ π pathway has a comparable height to that corresponding to the $S = 2$ σ pathway as long as there is no significant steric hindrance from ligand crowding preventing the perpendicular access of the C–H bond [46, 142]. Finally, the two-state $S = 1/S = 2$ pathway for HAA can be operative for the $S = 1$ NHFe^{IV}=O systems that contain bulky ligands and thus the only access for the C–H bond is along the Fe=O axis, favoring the $S = 2$ σ attack [139, 146].

Concerning the synthetic non-heme ligand design, the pioneering works of Wieghardt and Que [147, 148] demonstrated that a non-heme non-enzymatic environment could support the iron–oxo active intermediate. Since then, a substantial effort has been directed to synthesizing and improving ligands for HAA, which opened a broad field for the joint experimental and theoretical efforts. The computational effort focused initially on model complexes. Baerends and co-workers noted the crucial importance of the energy of the acceptor orbital. In a series of studies on simple complexes with H_2O and NH_3 ligands, they were able to tune the energy of the acceptor orbital by the nature of the axial ligand and adjust the HAA barriers [149, 150], while the efficiency of iron over other transition metals was also demonstrated [151]. A recent contribution [152] offers a modification over the popular TMC ligand via an ethylene bridge that constricts the monodentate ligand (MeCN) to the equatorial position with respect to the Fe–oxo bond. Computational analysis attributes the manifested increase in reactivity in the tested HAA and oxygen atom transfer (OAT) reactions to the increased spin density of the oxo oxygen in the modified ligand, in a typical high-spin reactivity scenario.

Another case of modification of a popular ligand was reported recently, simulating the histidine environment of the enzyme by replacing one or two of the pyridyl moieties of N4Py (*N*,*N*-bis(pyridylmethyl)-*N*-bis(2-pyridyl)methylamine; see Fig. 2) by benzimidazole [153]. The HAA reactivity is increased by each replacement—weakening of the ligand field opens the high-spin pathway—and the DFT calculations are able to follow this trend with respect to the high-spin barriers. It is evident from the few works selected above and the several mentioned throughout Sect. 3 of the current minireview that theory can be utilized not only to rationalize the experimental findings but also to assist in the design of ligands tuned for HAA. An invaluable tool is the thermodynamic driving force described by the

Bordwell–Evans–Polanyi linear relations (BEP, vide infra) [154]. This relation was confirmed in a series of heme and non-heme complexes [155] and in a meta-analysis of thirteen literature studies where high-spin states are found more reactive, but only in 70 % of the cases [156].

Complementing the predictive ability of the BEP linear relations but from an electronic structure perspective, a relation between a simple descriptor of the initial complex and the HAA reactivity was established [88]. The energies of the acceptor orbitals of a diverse, extensive set of iron–oxo complexes were found to correlate linearly with the reaction barrier of the hydrogen abstraction, regardless of charge/spin ground state or solvation. As in the case of the BEP relations, low/intermediate spin reaction pathways were shown to be as effective. The established correlation, since it relies on obtaining the electronic structure of only the initial complex, allows for a fast screening of potential catalysts.

General strategies for HAA ligand design stemming from the above and other computational studies include the requirement to utilize a weak equatorial and the weakest possible axial ligand field, as well as the employment of non-polar solvents. These were dominant criteria in the aforementioned examples of improving the reactivity of existing iron–oxo complexes [152, 153] (i.e., blocking the axial position for acetonitrile and employing weaker donor ligands).

Mononuclear ferric–hydroperoxo active site:
$C\text{–}H + HOO\text{–}Fe^{III} \rightarrow C^{\bullet} + H_2O + O = Fe^{IV}$

The low-spin ($S = 1/2$) Fe^{III}–OOH structure was experimentally identified as the "activated form" of an anticancer metallopeptidic agent, bleomycin, and shown to be reactive towards HAA from DNA [45]. On the other hand, the high-spin ($S = 5/2$) Fe^{III}–OOH intermediate, proposed to be formed in Rieske dioxygenases (RDO) [157–159], should have oxidant ability in electrophilic aromatic substitution reactions (note that alternative intermediates in RDO were also proposed [160, 161]). While information on the biological $NHFe^{III}$–OOH active sites are limited (e.g., direct detection for the $S = 5/2$ Fe^{III}–OOH intermediate remains elusive), considerable advances have been achieved in experimental and theoretical chemistry of low-weighted $NHFe^{III}$–OOH species [6, 9, 135].

Recently, Solomon and co-workers investigated two synthetic $S = 1/2$ (N4Py)Fe^{III}–OOH and $S = 5/2$ (TMC) Fe^{III}–OOH complexes in an attempt to elucidate differential electronic structure (spin-state) effects on reactivity. Indeed, they showed that both $S = 1/2$ and $S = 5/2$ systems are capable of HAA (with a comparable barrier height) but the reaction coordinates are very different [11]. In the comparative study, the B3LYP method reproduced the experimental activation free energies and enthalpies obtained from Eyring plots, giving credence to the computational findings. The HAA transition state (TS) at the $S = 1/2$ surface was calculated to be late in the O–OH bond length (2.38 Å), whereas the C–H bond stayed intact (1.12 Å). Electronically, the TS corresponds to a hydroxyl ($OH^{\bullet}$) attack on the C–H bond. At the same time, the HAA TS at the $S = 5/2$ surface was characterized as early in O–OH (1.79 Å) and further along in C–H coordinate (1.17 Å), with an electron partially transferred from the substrate to the Fe–OOH moiety. From these analyses, it has been shown that the HAA reactivity of the $S = 5/2$ state is clearly dependent on the substrate properties, which is not the case for the $S = 1/2$ system. Indeed, calculations revealed a strong linear dependence of the activation energy for the $S = 5/2$ HAA reaction on the substrate ionization potential (and C–H bond strength) that was not observed for the $S = 1/2$ HAA reactions. Thus, the high-spin $NHFe^{III}$–OOH active site was proposed to be more effective in controlling biochemical and environmental processes than their low-spin cognates (see also Fe^{III}–OOH in Sect. 3.3) [11].

Mononuclear ferric–superoxo active site:
$C\text{–}H + {}^{-\bullet}OO\text{–}Fe^{III} \rightarrow C^{\bullet} + HOO\text{–}Fe^{III}$

A mononuclear Fe^{III}–$OO^{\bullet-}$ intermediate, capable of substrate C—H bond activation, has been proposed for enzymes such as IPNS [162] and HEPD [163], while in other mononuclear NHFe enzymes, it is responsible for the electrophilic oxidation of an aromatic ring instead of HAA [164] (the $NHFe_2$ MIOX is the only enzyme proved to use Fe^{III}–$OO^{\bullet-}$ for HAA—more in Sect. 3.2.4). Among the NHFe model complexes, the first synthetic (TAML-supported) non-heme $Fe^{III}O_2^{\bullet-}$ structure (with $O_2^{\bullet-}$ in a side-on binding mode; TAML: tetraamido macrocyclic ligand; see Fig. 2) was crystallographically defined only as late as in 2014 [165]. This synthetic system was shown to undergo both an aliphatic C—H activation and nucleophilic oxidation reaction. In any case, due to the limited body of experimental data, theoretical insight on reaction mechanisms that would involve the ferric–superoxo structure are, therefore, of particular importance.

In the study on IPNS, Brown et al. [162] used a spectroscopically calibrated DFT method (the BP86 functional with 10 % HF exchange admixture) to describe the electronic structure of the ferric superoxo site as a high-spin ($S = 5/2$) Fe^{III} center anti-ferromagnetically coupled to the $O_2^{\bullet-}$ moiety, giving rise to a total spin of $S = 2$ (the quintet state was also reported for the ferric superoxo intermediate of other enzymes: 2,3-HPCD [164] and cysteine dioxygenase (CDO) [166] although the $S = 2$ state in CDO was suggested to arise from the ferromagnetic coupling

of $O_2^{\bullet-}$ to $S = 3/2$ Fe^{III}; note also that both 2,3-HPCD and CDO are not operative in HAA but rather in electrophilic aromatic substitution and S-oxidation, respectively). DFT calculations also revealed that substrate (thiolate) binding to the iron center in IPNS makes the formation of this ferric superoxo structure exergonic. The formation of the product of dioxygen activation by Fe^{II} would be otherwise unfavorable in the resting H_2O-bound form. The thermodynamic driving force was, therefore, attributed to the stabilizing effect of thiolate charge donation. In addition, the description of how substrate charge donation influences the FMO of the $S = 2$ Fe^{III}–$OO^{\bullet-}$ unit and thus makes it well-oriented for selective HAA was provided. Despite all these findings, the energetics of the HAA reaction by the $S = 2$ Fe^{III}–$OO^{\bullet-}$ site (and the subsequent steps of the catalytic cycle) was not evaluated in Ref. [162].

This was done by Lundberg et al. [167] who modeled the whole catalytic cycle of IPNS using the B3LYP/MM approach and calculated the free-energy barrier of HAA to be ~12 kcal mol^{-1} (the experimentally derived value is ~17 kcal mol^{-1}), which is associated with the $S = 2$ Fe^{III}–$OO^{\bullet-}$ species. However, it is noticeable that B3LYP favors the septet ($S = 3$) as the ground spin state, which is much less reactive towards HAA. The same issue with the ground spin state of the Fe^{III}–$OO^{\bullet-}$ unit was also brought up in the QM(B3LYP) and QM(B3LYP)/MM study on the reaction mechanism of the HEPD system [168]. Nevertheless, the cited work provided a plausible mechanistic picture of the catalytic transformation of two different substrates in HEPD, both activated through HAA by $S = 2$ Fe^{III}–$OO^{\bullet-}$.

HAA reactivities of Fe^{III}–$OO^{\bullet-}$ versus Fe^{IV}=O species were examined and compared at the DFT level of theory in Ref. [169]. This comparison included both heme and non-heme model complexes and covered different binding modes of the $O_2^{\bullet-}$ moiety. Their results showed that Fe^{III}–$OO^{\bullet-}$ is not, in general, a better oxidant than ferryl compounds and in fact its oxidation power strongly depends on the HAA reaction energy. Namely, they showed that for both types of oxidants, the HAA activation energies correlate well with reaction energies, thus obeying the BEP principle (see also Sect. 3.2.5). For a given reaction energy, the HAA barrier is smaller for ferric superoxo than for ferryl by ~7 kcal mol^{-1} in average. Finally, the spin-state effects of Fe^{III}–$OO^{\bullet-}$ on HAA reactivity were investigated, validating the $S = 2$ state to be more reactive than $S = 1$ or $S = 3$. Specifically for the $S = 2$ state, Chen et al. employed the B3LYP and CCSD(T) methods to demonstrate [132] that the nature of magnetic interactions between the superoxyl radical and ferric ion depend on the FeOO angle (i.e., the side-on vs. end-on binding mode corresponding to the ferromagnetic vs. antiferromagnetic configuration).

H-atom abstraction by binuclear $NHFe_2$ active sites

The presence of diferrous centers in $NHFe_2$ active sites makes strategies for the O_2 activation pathways very complex and mostly different from those adapted by mononuclear NHFe biocatalysts (see also Sect. 3.1). In brief, the common theme for most of $NHFe_2$ enzymes is the two-electron reduction of dioxygen by the $Fe^{II}Fe^{II}$ center that produces low-spin ($S = 0$) peroxo-bridged biferric intermediates ("**P**" intermediates). Frequently, the **P** intermediate can be further converted to other intermediates, such as the bis-μ-oxo $Fe^{IV}Fe^{IV}$ intermediate ("**Q**" intermediate) of methane monooxygenase (MMO), which is thought to initiate the $CH_4 \rightarrow CH_3OH$ transformation by HAA. Alternatively to MMO, the **P** intermediate in ribonucleotide reductase (RNR) is converted to an oxygenated $Fe^{III}Fe^{IV}$ (so-called **X**) intermediate, which is responsible for the homolytic O─H cleavage in the tyrosine residue [170].

Another $NHFe_2$ enzyme (structurally related to MMO and RNR) that performs the catalytic transformation of a substrate through an HAA process is the soluble Δ^9 desaturase (Δ^9D), catalyzing the dehydrogenation of the stearoyl substrate to oleic acid. In Δ^9D, the **P** intermediate has been structurally characterized by correlating QM(DFT)/MM calculations with spectroscopic data and shown to be unreactive towards HAA from the substrate [23]. This initiated an extensive computational search for an intermediate that can be formed from **P** (by structural rearrangement or/and protonation or/and water binding or/and $1e^-$ reduction) and can attack effectively the aliphatic C─H bond of the stearoyl substrate [23, 85]. In Ref. [23] the authors also pointed out discrepancies in the prediction of energetics of the OO bond cleavage step from **P** using different DFT functionals. For this reason, the large active-space multireference DMRG-CASPT2 method, using for the QM(DFT)/MM structural models, was employed for the calculation of energetics of nine different reactions, potentially relevant for HAA or a step that would precede HAA [85]. This led to the following suggestion: the **P** ($S = 0$ 1,2-μ peroxide $Fe^{III}Fe^{III}$) intermediate is, upon protonation of the peroxide moiety, transformed into low-spin ($S = 0$) 1,1-μ OOH^- $Fe^{III}_{(S=5/2)}Fe^{III}_{(S=5/2)}$ that is potent to abstract the first H-atom from the substrate. In addition, the performance of several popular DFT functionals was calibrated against the "reference" DMRG-CASPT2 values (admitting that it can be a matter of debate whether (DMRG-)CASPT2 may develop into a true benchmark method for strongly correlated systems, analogously to what the CCSD(T) method is in the realm of smaller closed-shell systems). It needs to be emphasized that the accuracy of all tested DFT functionals remained modest (TPSSH, B3LYP, M06) or poor (B2PLYP, M06L, BP86). In addition, it is important to note that the full reaction coordinate for C─H bond activation by 1,1-μ

OOH^- $Fe^{III}Fe^{III}$ was found to be an unsolved issue, i.e., most DFT-based calculations predict the hydride (H^+,$2e^-$) abstraction (with two-electron transfer occurring after TS) instead of HAA. This would lead to hydroxylation of the substrate instead of desaturation. The DMRG-CASPT2 results were inconclusive since the comparison of hydride versus H-atom abstraction energetics was carried out for the reactant-like TS structure. All these intricacies associated with DFT methods support an urgent requirement for large-scale multireference methods (discussed in Sect. 2.3) that would allow a quantitatively correct electronic structure description and hence energetics in binuclear NHFe systems.

An $NHFe_2$ enzyme that uses a "less common" mixed-valent $Fe^{II}Fe^{III}$ active site for O_2 activation [171] and does not involve a peroxy-level intermediate prior to the HAA step is MIOX, catalyzing the oxidative conversion of *myo*-inositol to D-glucuronate [172]. Instead, a superoxo-diferric species (the so-called **G** intermediate) was suggested as the key oxygenated NHFe intermediate activating the substrate through HAA [140]. Hirao and Morokuma predicted geometric/electronic properties of the **G** intermediate and its HAA reactivity using QM(B3LYP)/MM modeling [173]. According to their calculations, the **G** intermediate can be characterized as an $S = 1/2$ side-on $O_2^{\bullet-}$ $Fe^{III}_{A\ S=5/2}Fe^{III}_{B\ S=5/2}$ complex (two Fe centers are anti-ferromagnetically coupled) but with the O_2 moiety being only partially reduced to superoxide. Nevertheless, such a complex could be competent for HAA with a barrier of ~18 kcal mol^{-1}, which is lower than the putative subsequent step involving the O–OH bond cleavage (this would be in line with measured steady-state kinetic isotope effect, KIE ~1).

Reduction potential/basicity correlated to H-atom abstraction reactivity

In the work of Sastri et al. [174], HAA reactivity of Fe^{IV}=O complexes was correlated with their reduction potentials. Within the series of TMC-supported Fe^{IV}=O cognates that differ by a ligand in the trans-axial position with respect to the oxo group, a surprising relationship between the HAA reaction rate and the reduction potential was found: the lower the reduction potential of the Fe^{IV}=O species, the higher the HAA reactivity. Along these lines, the work reported by Lacy et al. [175] proved that both $S = 5/2$ $(H_3buea)Fe^{III}O$ and $S = 2$ $(H_3buea)Fe^{IV}O$ complexes (H_3buea^{3-} = an urea-based tripod; see Fig. 2) with very low reduction potentials (i.e., −0.9 V and lower than −2.0 V vs. $Fc^{0/+}$, respectively) can abstract an H-atom from sufficiently weak organic substrates. Following Mayer's protocol [154], the strength of the O–H bond in the HAA product (e.g., Fe^{III}–OH) can be expressed as a function of the reduction potential and basicity of the oxidizing agent (e.g., Fe^{IV}=O). From the thermodynamic point of view, the stronger O–H bond reflects the stronger propensity of an oxidant for H-atom (H^+,e^-) abstraction from a substrate. Then, this stronger propensity for HAA implies the faster HAA rate according to the BEP principle. The BEP principle was invoked in many kinetic studies on NHFe species, demonstrating a correlation between a decreased C–H bond strength and an increased HAA reaction rate—see for example refs [176, 177]. Thus, high basicity can explain why some NHFe complexes are competent for HAA despite their very low reduction potential (and vice versa). Indeed, the importance of basicity contributions to the HAA reactivity was revealed for the thiolate and heme-bound Fe^{IV}=O center in cytochrome P450 [178]. It is also reasonable to expect such a basicity-driven HAA reaction to be operative in some non-heme iron enzymes that could use a low reduction potential to avoid unwanted oxidations of the fragile protein structure.

In a theoretical work, Usharani et al. [179] linked the basicity of the Fe^{IV}=O oxidant with a mechanism for HAA, i.e., the concerted H-atom transfer (HAT) versus the proton-coupled electron transfer (PCET). Using valence bond-based arguments, they concluded that a less basic oxidant exhibits a higher oxyl character on the oxo group that is required for the more concerted HAT (more homolytic) process. In contrast, a more basic oxidant tends to cleave bonds more heterolytically (through PCET) and is, therefore, operative for N–H, O–H or more acidic C–H bonds. For an understanding of PCET processes (among which HAT is considered as a specific case) we recommend Refs. [180, 181].

As described above, the reduction potentials and the acidity constants are the key thermodynamic quantities that are directly related to HAA reactivity. Despite their importance in $NHFe_{(2)}$ chemistry, their calculations remain challenging due to large environmental effects that have to be properly described. This can be achieved by the inclusion of explicit solvent molecules [182] and/or remote parts of a protein through the QM/MM(+FEP) scheme [183], but this also usually requires an extensive sampling of the conformational space. On the other hand, the implicit solvent models are simplistic and do not account sufficiently for solvation-energy differences between protonated and deprotonated or oxidized and reduced species [184]. It is noticeable that Bím et al. [89] recently suggested an implicit solvent-based protocol for the calculation of one-electron reduction potentials of multiple-charged species. In their approach, the reduction potential of a charged species is calculated by means of the reduction potential of its neutralized (protonated/deprotonated) cognate, employing one or several H-atom addition/abstraction thermodynamic cycles. This includes a separation of one-electron reduction from protonation/deprotonation through the temperature dependence.

Kinetic isotope effect

Many inorganic and enzymatic reactions involving HAA exhibit a large primary kinetic isotope effect (KIE > ~10), such as KIE = 35 observed in NHFe taurine dioxygenase [185] or KIE = 60 in NHFe prolyl-4-hydroxylase [186], which usually indicates significant tunneling effects on reaction dynamics. Consequently, a large primary KIE serves for evincing HAA as the rate-determining step in a reaction and is, therefore, very useful for modeling a reaction mechanism (experimental KIE data are mostly reflected in calculations by searching for a mechanism in which the HAA step would be associated with the highest free-energy barrier along a reaction coordinate). However, direct KIE calculations remain a very difficult task. The simplest approximations to KIE that incorporate Wigner or Bell tunneling corrections to the Eyring's transition state theory (TST) are quantitatively incorrect for reproducing large KIEs [187, 188].

Recently, Shaik and co-workers [188] calculated tunneling contributions to HAA reactivity within the series of the TMC-supported Fe^{IV}=O complexes by employing the Eckart method [189, 190] in combination with TST in attempt to rationalize the "anti-electrophilic" trend [46] in HAA (i.e., the stronger an electron-donating axial ligand X in the TMC-supported X–Fe^{IV}=O complex is, the faster the HAA reaction) [188]. Note that these $S = 1$ NHFe^{IV}=O systems undergo a two-state $S = 1/S = 2$ σ pathway (see Sect. 3.2.1) [139, 146]. To evaluate tunneling effects, the Eckart barrier function (EF) was fitted to a "one-dimensional" adiabatic barrier (calculated along an intrinsic reaction coordinate), and the tunneling transmissions (τ) were then calculated by integrating an energy-dependent penetration probability through EFs. As a result, the TST-determined activation barrier is effectively lowered by $RT \times \ln\tau$. Their calculated KIEs correlate with the barrier widths, i.e., a larger barrier width is reflected by a lower tunneling effect on KIE and thus a smaller KIE value. These calculations were found to provide results comparable to experimental data (e.g., KIE_{calcd} = ~14 vs. KIE_{expt} = 10 for $(CH_3CN)(TMC)Fe^{IV}$ = O; KIE_{calcd} = ~25 vs. KIE_{expt} = 17 for (azide)(TMC)Fe^{IV}=O). The authors also predicted that the π-controlled $S = 1$ HAA pathway would be associated with much larger KIE.

However, the "larger-width-smaller-KIE" correlations from Ref. [188] seem to contrast with calculations of Hammes-Schiffer [191] who studied the HAA reaction in the mononuclear NHFe soybean lipoxygenase using non-adiabatic PCET theory (i.e., C–H + HO–Fe^{III} → $C^{\bullet}$ + H_2O–Fe^{II}; note that unlike the majority of known NHFe enzymes that activate dioxygen for attack of a substrate, lipoxygenase activates a substrate for the attack of O_2; see Fig. 6). Applying this theory, Hammes-Schiffer and co-workers [191] reproduced the experimental value of the KIE as well as its temperature dependence (applicability of non-adiabatic formulation of the theory was tested for HAA in this system). Moreover, a non-intuitive dependence of KIE on the equilibrium distance between $C_{[substrate]}$ and $O_{[FeOH]}$ was shown: a larger C–O separation, implying a larger barrier width for H-atom transfer, leads to a larger KIE value (this dependence reflects different overlaps between the reactant and product proton/deuteron vibrational wave functions). From the Hammes-Schiffer's PCET theory, "larger-width-larger-KIE" predictions can be expected as long as other parameters (e.g., the frequency associated with donor–acceptor distance motion) are fixed and only ground vibronic state contributions to the rate constant are important [191]. Such a prediction was experimentally verified for the NHFe lipoxygenase and its single- or double-mutant forms [192, 193].

From a brief discussion above, it is clear that the KIE (and its temperature dependence) has a potential of being a sensitive probe of some structural/mechanistic details about the rate-determining HAA step (e.g., separation and/or orientation of the substrate C–H bond with respect to a reactive NHFe unit, spin-state effects, etc.). However, it is fair to admit that quantitative primary KIE evaluations are extremely challenging for quantum chemistry due to the requirements on the accuracy of calculated reaction barriers, their curvatures (widths) and hydrogen/deuterium nuclear quantum effects.

Modeling oxygen atom transfer reactions

As we discussed in the previous sections, many classes of NHFe enzymes exhibit considerable diversity in their biological functions. We already mentioned the importance of different oxygenated intermediates for the activity of NHFe enzymes toward HAA from organic substrates. In this section, we will discuss the electrophilic oxidation reactivities of such intermediates, focusing mainly on the OAT reactions (i.e., direct electrophilic attack of an O-atom on organic substrates). Enzymes that are able to incorporate oxygen into the substrate structures play a crucial role in several important metabolic pathways, converting aliphatic and aromatic compounds into alcohols or epoxides, thiols to sulfenic or sulfinic acids, sulfides to sulfoxides, phosphines to phosphine oxides, etc. To understand the possible roles of the key oxygenated intermediates as active oxidants, many low-weighted biomimetic models were synthesized [135, 136].

Mononuclear ferryl active site

The $S = 2$ Fe^{IV}=O intermediate was trapped in several pterin-dependent hydroxylases (i.e., tyrosine [194], phenylalanine [195], or tryptophan [196, 197] hydroxylases).

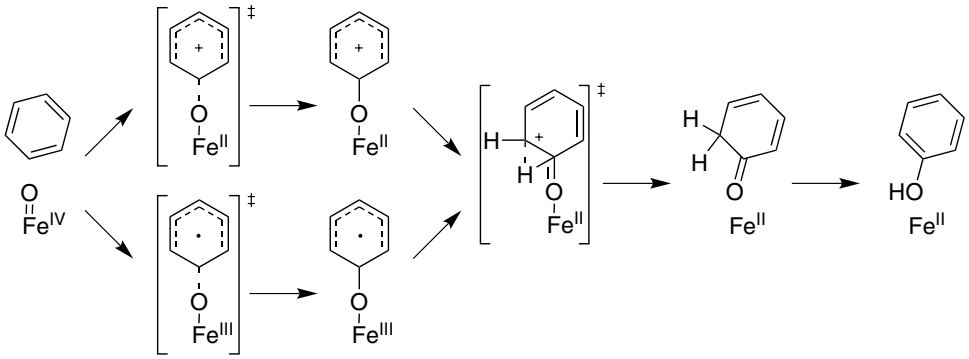

Fig. 8 Two mechanisms of electrophilic aromatic substitution: a single-step two-electron transfer (*upper part*) vs. two sequential one-electron transfers (*lower part*)

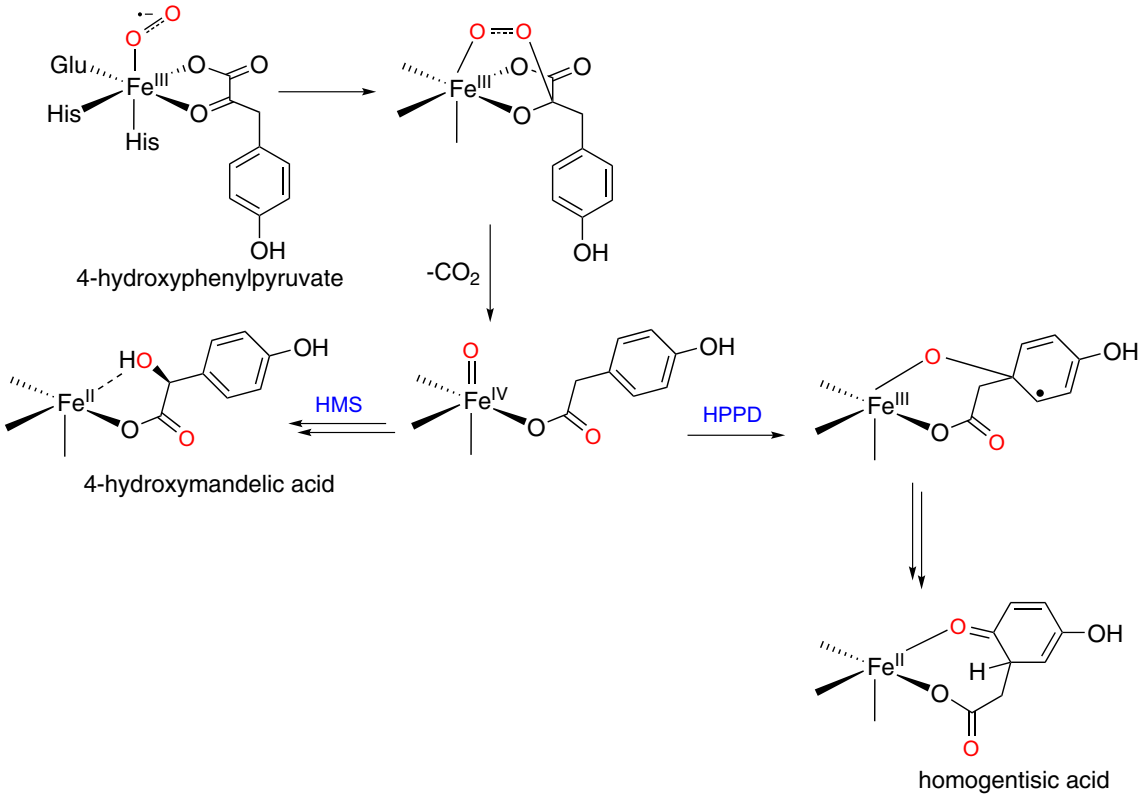

Fig. 9 Key steps of the reactions of the HMS and HPPD enzymes

These enzymes hydroxylate the aromatic substrates by the electrophilic substitution mechanism that proceeds formally through $2e^-$ transfer from the oxo group to Fe^{IV} and direct OAT as depicted in Fig. 8.

The electrophilic aromatic substitution mechanism was also suggested for 4-hydroxyphenylpyruvate dioxygenase (HPPD) [144, 198]. HPPD together with 4-hydroxymandelate synthase (HMS) belong to the α-ketoacid dependent dioxygenases that have structurally similar active sites but differ considerably in reactivity. While HMS performs benzylic hydroxylation of 4-hydroxyphenylpyruvate (HPP), HPPD is responsible for aromatic hydroxylation of the same substrate (see Fig. 9). According to DFT calculations performed on small model systems [144, 198, 228], dioxygen activation in both HMS and HPPD produces the $S = 2$ Fe^{IV}=O intermediate capable of OAT (in HPPD) or HAA (in HMS), depending on the substrate orientation with respect to the Fe^{IV}=O moiety. In particular, the spectroscopy-based work of Neidig et al. [144] provided a detailed mechanistic insight into the OAT versus HAA reaction. Notably, the OAT-controlled σ-attack on substrate in HPPD leads to an $S = 5/2$ spin state on the generated Fe^{III} center, whereas HAA-controlled π-attack in HMS gives rise to $S(Fe^{III}) = 3/2$ (the notion of π vs. σ attack is discussed in

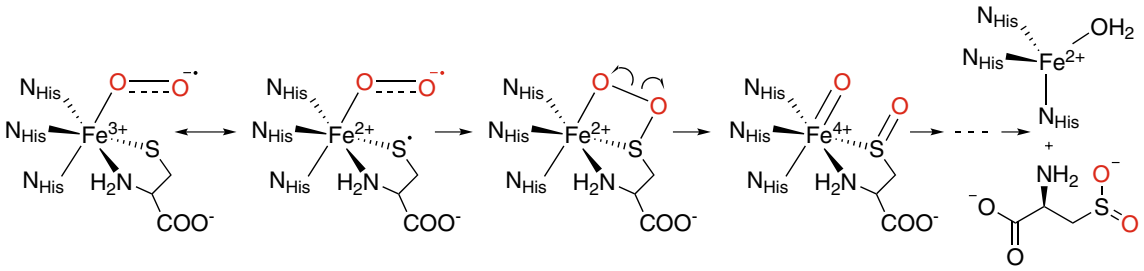

Fig. 10 Proposed mechanism of CDO [114]

Sect. 3.2.1). A recent QM/MM study [229] extended the knowledge about the mechanism of aromatic and benzylic hydroxylation in HPPD and HMS by completing their catalytic cycle.

An Fe^{IV}=O intermediate competent for OAT was also proposed for CDO [199]. CDO catalyzes S-oxygenation of cysteine (RS^-) to cysteine sulfinic acid ($R\text{-}SO_2^-$) through a mechanism that has been suggested as follows (Fig. 10). First, the cysteine-bound Fe^{III}–superoxo intermediate, which was observed experimentally [200], initiates the electrophilic attack on the cysteinyl sulfur lone pair with a subsequent $1e^-$ transfer from the superoxide back to Fe^{III} center, resulting in the formation of an $S = 2$ four-membered (Fe^{II}–O–O–S) ring intermediate [111, 114]. This intermediate then undergoes the O–O bond cleavage that produces the Fe^{IV}–oxo moiety and the sulfenic intermediate. A spin-crossover was suggested prior to O–O bond cleavage that would lead to the $S = 1$ state for the Fe^{IV}–oxo and was calculated to be significantly lower in energy (8.3 kcal mol^{-1}) than the $S = 2$ state (B3LYP) [111]. However, these findings contrast with the $S = 2$ ground spin state that was observed for all spectroscopically characterized Fe^{IV}–oxo intermediates. Thus, the computationally proposed $S = 1$ state for the Fe^{IV}–oxo intermediate in CDO would be very unique, raising a question about its functional role in a subsequent OAT step that completes the oxidation of Fe-bound sulfur. In the study of biomimetic complexes, it was demonstrated that ferryl undergoes OAT through different mechanisms, depending on the ground spin state (vide infra) [146].

It was earlier predicted by the theoretical calculations [142, 201] that $S = 2$ Fe^{IV}=O species are more reactive in the oxidative reactions than their $S = 1$ analogs. It should be, however, noted that the direct experimental evidence is still lacking. While the $S = 1$ Fe^{IV}=O species are common in biomimetic NHFe chemistry, the $S = 2$ complexes were synthesized only recently [136]. Moreover, it was demonstrated that $S = 2$ state models show only comparable (or even lower) reactivity towards OAT or HAA [202–205]. These observations emphasized the need for the correlation of reactivity with electronic structure as well as the geometric and steric properties of a complex. The study of Sastri et al. [174] provided a comprehensive correlation between the electronic structure properties (reflected by the reduction potentials) and reactivity. In the context of HAA reactivity, this was discussed in the Sect. 3. Analogously, the OAT reactivity that involves two-electron transfer from substrate to the iron center was probed in a series of $S = 1$ $[Fe^{IV}(O)(TMC)(X)]^{n+}$ and $[Fe^{IV}(O)(TMCS)]^+$ species (with X = 1-$NCCH_3$, 1-$OOCCF_3$ and 1-N_3; TMCS = 1-mercaptoethyl-4,8,11-trimethyl-1,4,8,11-tetraazacyclotetradecane; see Fig. 2) by investigating the oxidation of PPh_3 to Ph_3PO. It was revealed that the decrease in electrophilicity of the axial ligand, which causes a decrease in the reduction potential of the complex, results in a decrease of OAT rates (the opposite trend was observed for HAA). B3LYP calculations further revealed that an increase in the electron-donating ability of axial ligands results in the decrease of the $S = 2/S = 1$ energy gap, which in turn suggested an increased availability of $S = 2$ for OAT reactivity (the $S = 2$ TS for OAT was found lower in energy than the $S = 1$ TS, suggesting the $S = 1 \rightarrow S = 2$ mechanism for OAT). The correlation between OAT rates and reduction potentials (or quintet-triplet energy differences) was found in other studies as well [16, 206, 207].

The systematic work of Wilson et al. [146] sheds additional light on OAT reactivity of $NHFe^{IV}$=O complexes, which was investigated (along with HAA reactivity) for two structurally related $[Fe^{IV}(O)(TMC)(CH_3CN)]^{2+}$ and $[Fe^{IV}(O)(TBC)(CH_3CN)]^{2+}$ species (TBC is 1,4,8,11-tetrabenzyl-1,4,8,11-tetraazacyclotetradecane, i.e., it has more bulky benzyl substituents attached to the cyclam scaffold; see Fig. 2). Unexpectedly, the rate was enhanced by two orders of magnitude for both HAA and OAT reactions of the TBC-supported complex (as compared to the complex with the TMC chelate). B3LYP calculations showed that the replacement of TMC by a more bulky TBC leads to a smaller energetic splitting between the $S = 1$ and $S = 2$ states of ferryl, making the $S = 2$ state more accessible for the TBC-supported complex. In addition, by inspecting the OAT reaction with the thioanisole substrate, the $S = 2$

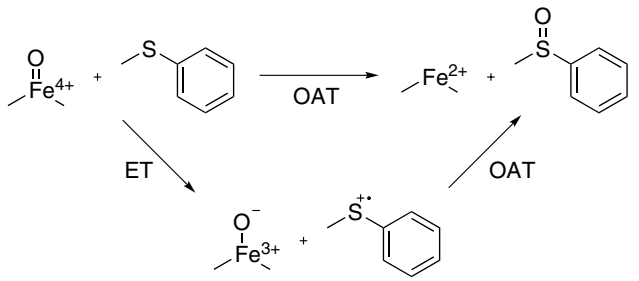

Fig. 11 Oxidation of thioanisole. Difference between direct OAT pathway (*upper part*) and outer sphere electron transfer pathway (*lower part*) [212]

transition state for OAT was found to be significantly lower in energy than the $S = 1$ TS. This is in line with the stabilization of the α-d_{z2} and hence increased axial reactivity in going from $S = 1$ to $S = 2$ $Fe^{IV} = O$. As a result, the electronic structure at the $S = 2$ TS is characterized as an early σ-attack (transfer of an α-electron into d_{z2}) that weakens both the Fe–oxo and trans-axial Fe–acetonitrile bonds, which in turn allows the Fe–oxo bond to move out of the cyclam plane and decreases the chelate steric hindrance for a "subsequent" β-electron transfer through a π-attack on the substrate. At the $S = 1$ TS, these σ- and π-attacks are more concerted, which is reflected by a much smaller distortion of the Fe–oxo bond from the cyclam plane, and thus larger chelate steric contributions to the barrier for the $S = 1$ OAT.

Interestingly, the complex $[Fe^{IV}(O)(13\text{-TMC})]^{2+}$ that differs only by having one less methylene group in the structure of 13-TMC as compared with TMC (see Fig. 2) exhibits larger than 10^5-fold reaction rate towards thioanisole sulfur oxidation than $[Fe^{IV}(O)(TMC)]^{2+}$ [208]. In line with observations for the series of TMC-supported complexes from Ref. [174], it is tempting to link the higher reactivity in OAT reactions with the higher reduction potential of the complex: for $[Fe^{IV}(O)(13\text{-TMC})]^{2+}$ and $[Fe^{IV}(O)(TMC)]^{2+}$, the reduction potentials were reported to be 0.61 and 0.39 V vs. SCE, respectively [208].

In 2010, Fukuzumi et al. [209] reported the crystal structure of $[Fe^{IV}(O)(TMC)]^{2+}$ complex with a bound Sc^{3+} ion to the oxo group that was shown to have stronger oxidizing capability than $[Fe^{IV}(O)(TMC)]^{2+}$ [210]. This again correlates with an increased OAT reaction rate [211]. As an alternative to metal cations, the presence of Brønsted acids in solution can also increase the OAT rate (i.e., the addition of $HClO_4$ to MeCN solution of $[Fe^{IV}(O)(N4Py)]^{2+}$ promotes sulfoxidation of the thioanisole by three orders of magnitude) [212]. To rationalize these observations, it was suggested that Lewis acid (Sc^{3+}) binding initiates sulfoxidation of the substrate sulfur by outer sphere electron transfer (lower part of Fig. 11), whereas a Brønsted acid ($HClO_4$) would contribute to a direct OAT mechanism (top part of Fig. 11) through the protonation of the oxo group in $[Fe^{IV}(O)(N4Py)]^{2+}$. Different mechanisms were attributed to differences in steric effects [212]. Nevertheless, more recent studies have shown that the assignment of the oxidation state of Fe–O–Sc^{3+} species was incorrect. DFT calculations carried out by Swart [213] suggested the formation of Fe^{III}–O–Sc^{III} species, which was also confirmed by spectroscopic methods [214]. These findings raise the question on how the Fe^{III}–O–Sc^{III} is formed from $[Fe^{IV}(O)(TMC)]^{2+}$. The Brønsted acid activation can be utilized in tuning of the first and second coordination sphere of the iron center in a design of biomimetic model complexes. Later, ferryl complexes with ligands possessing pendant arms capable of hydrogen bonding to the Fe^{IV}=O group were synthesized [215, 216] and shown to have significantly enhanced OAT reactivity. However, the detailed analysis of these effects on reactivity of such complexes was not provided.

Mononuclear ferric–peroxo and ferric–hydroperoxo active site

The $S = 5/2$ ferric–hydroperoxo intermediate was proposed to be competent for an electrophilic oxygenation reaction (aromatic hydroxylation) in RDO [19, 158, 159]. Nowadays, two competing possibilities for the role of $S = 5/2$ ferric─hydroperoxo in RDO are suggested: (i) the Fe^{III}–OOH species serves directly as the electrophilic oxidant; [158, 217] (ii) the Fe^{III}–OOH species is converted to either an Fe^{IV}=O intermediate through homolytic O–O bond cleavage [218] or an Fe^{V}=O intermediate through heterolytic O–O bond cleavage [219–221]. Many early studies claimed that the Fe^{IV}=O or Fe^{V}=O intermediates are preferable due to the lack of the experimental/theoretical evidence for OAT reactivity of the Fe^{III}–OOH species in electrophilic oxidations. In an attempt to shed light on this problem, Ansari et al. [222] computationally investigated possible HAA vs. OAT reactivities of three oxidants Fe^{III}–OOH, Fe^{IV}=O, Fe^{V}=O (derived from the $[Fe^{II}(TPA)(CH_3CN)_2]^{2+}$ complex). The direct OAT has been proposed as a more likely mechanism of action considering the *ortho*-hydroxylation of aromatic compounds. Based on their calculations, they concluded that the Fe^{V}=O intermediate is more reactive toward OAT than Fe^{IV}=O, while Fe^{III}–OOH was found to be a rather sluggish oxidant in the studied aromatic hydroxylation.

Similar results were obtained experimentally [223] for the nucleophilic (deformylation of aldehydes) and electrophilic (oxidation of sulfides and olefins) reactivities of in situ-generated non-heme Fe^{III}–OOH complexes with N4Py, Bn-TPEN, TMC and TPA ligands (Bn-TPEN = *N*-benzyl-*N*,*N*′,*N*′-tris(2-pyridylmethyl)-1,2-diaminoethane; see

Fig. 2). No reactivity was observed, and it was assumed that the Fe^{III}–OOH complexes cannot be used either in nucleophilic reactions or in electrophilic oxidations. The electrophilic oxidation was ruled out also in the case of ferric–peroxo species (i.e., alkylperoxo species [(TPA) Fe^{III}–(OOtBu)]$^{2+}$ [224]). Based on B3LYP calculations, it was concluded that the active oxygenation agent is an $S = 1$ Fe^{IV}=O system, which is generated through O–O bond homolysis of $S = 1/2$ Fe^{III}–OOR species. The calculations revealed a lower energetic barrier for the O–O bond activation of Fe^{III}–OOR in comparison with direct OAT to organic substrates (~23 kcal mol^{-1} for the O–O activation vs. >25 kcal mol^{-1} barrier for direct ethylene epoxidation). It is noteworthy that none of these complexes was stable, and detailed characterization is, therefore, lacking. Goldberg prepared the rare thiolate-ligated $S = 1/2$ [Fe^{III}([15]aneN_4–2H)(SC_6H_4-*p*-Cl)(OOH)]$^+$ species (see Fig. 2) [225]. Neither was this complex reported as reactive towards PPh_3 oxidation.

A considerable progress was achieved after the isolation and characterization of a side-on Fe^{III}–peroxo complex [Fe^{III}(TMC)(OO)]$^+$ [226]. It allowed the generation and characterization of all key species (Fe^{III}–peroxo, Fe^{III}–hydroperoxo and Fe^{IV}–oxo) within one host chelate, including the investigation of their mutual conversion and their reactivities. The peroxo complex was converted to the $S = 5/2$ end-on hydroperoxo complex [Fe^{III}(TMC)(OOH)]$^{2+}$, and it was proved that the Fe^{III}–hydroperoxo species is highly reactive in deformylation of aldehydes and has similar reactivity to the Fe^{IV}–oxo complex in C–H bond activation (which is in contrast with previous findings that predicted no reactivity of Fe^{III}–hydroperoxo in electrophilic and nucleophilic reactions [222–225]). In addition, Nam et al. [131] provided experimental evidence that $S = 5/2$ [Fe^{III}(TMC)(OOH)]$^{2+}$ is active also in oxidation of sulfides to sulfoxides. Moreover, based on the reaction with *p*-substituted thioanisoles, it was suggested that the hydroperoxo group shows electrophilic character, comparable with the Fe^{IV}–oxo species, and that oxidation of sulfides occurs through OAT. These experimental findings were complemented by B3LYP calculations that allowed to formulate a comprehensive mechanistic picture of the OAT process. According to these calculations, sulfoxidation proceeds on $S = 5/2$ surface via heterolytic O–O bond cleavage. Contrary to that, the $S = 1/2$ reaction trajectory follows a homolytic O–O bond cleavage but with a prohibitively large activation barrier (~32 kcal mol^{-1}). Indeed, no OAT-driven oxidation of sulfides was observed for the $S = 1/2$ hydroperoxo complex [Fe^{III}(N4Py)(OOH)]$^{2+}$ as opposed to OAT reactivity of $S = 5/2$ [Fe^{III}(TMC)(OOH)]$^{2+}$.

Recently, the capabilities of superoxide reductase (SOR) in nucleophilic and electrophilic oxidations through an $S = 5/2$ ferric–hydroperoxide intermediate were also investigated [227]. It was convincingly shown that SOR is able to react with aldehydes in deformylation reactions. In addition, its sulfoxidation was further demonstrated to proceed in the presence of SOR and 1 molar equiv. of H_2O_2.

Reaction selectivity

The iron–oxygen species generated in $NHFe_{(2)}$ enzymes are potent oxidants, and they are, at least in principle, capable of reacting with the substrate at various sites. The initially formed reactive intermediates, quite often substrate-centered radicals, may also have more than a single channel for further transformation. With their native substrates, enzymes typically show exclusive reactivity toward one product, and much is to be learned about how they achieve such excellent control over the outcome. The involvement of highly reactive species suggests that computations can prove essential in providing detailed insight into the selectivity-determining factors. This task is, however, challenging due to the necessity of taking into account a number of subtle interactions to a good accuracy to arrive at a realistic model, which can withstand thorough experimental tests (e.g., using mutated enzymes and alternative substrates).

Chemoselectivity

One excellent opportunity to study the effects governing selectivity is provided by the pair of NHFe enzymes HPPD and HMS (both defined in Sect. 3.3.1). Both belong to the family of α-KG-dependent dioxygenases and share the substrate, HPP, which as a ketoacid also serves as the surrogate of α-KG. The substrate-bound complex was found to be very similar in these systems [144], and following initial oxygen activation according to the established scheme of α-KG-enzymes, the reactions arrive at the common Fe^{IV}=O intermediate with complexed 4-hydroxyphenylacetic acid (see Figs. 4, 9). At this point, the reaction pathways diverge; in HPPD, the attack on the aromatic ring followed by migration of the carboxymethyl substituent leads to 2,5-dihydroxyphenylacetic acid (homogentisic acid), while in HMS, benzylic C–H abstraction and OH rebound provide the 4-hydroxymandelic acid product (Fig. 9). Detailed MD and QM/MM studies by Borowski et al. [228, 229] identified several key second sphere residues that, using H-bonding and steric bulk, stabilize different orientations of the 4-hydroxyphenylacetic acid toward the oxidant, leading to different favored pathways in the two cases. The results were in line with mutagenesis experiments on HPPD. Nevertheless, besides protein effects, other factors may also be at play. In these enzymes specifically, and in $NHFe^{IV}$=O species in general, there seems to be an intrinsic preference toward aliphatic hydroxylation [229],

particularly when compared with Fe^{IV}–oxo–porphyrin radical systems [230]. The high electron affinity (opposed by the lower pK_a to yield comparable BDE_{OH} values) was suggested to be responsible for this trend.

The selectivity-determining step may seem to occur following the initial substrate attack. Such is the case of the Fe-α-KG-dependent halogenase SyrB2, where the substrate, having undergone C–H abstraction by Fe^{IV}=O, could rebound either to the OH or to the Cl ligand of the iron, giving rise to a hydroxylated or halogenated product (see Fig. 3). Following seminal experiments on this system [231], calculations revealed a more complicated picture indicating that the selectivity arises earlier on. It was shown that positioning of the substrate and H-bond interactions of the incipient OH lead to the selection of a C–H abstraction reaction channel that brings the newly formed substrate radical into the proximity of the chloro ligand [44, 232]. Recent experiments fit well into the overall picture [233]. At the same time, it seems that intrinsic properties of the metal complex may also play a role here, as it was found that the synthetic $[Fe^{IV}(O)(TPA)Cl]^+$ complex has an appreciable preference toward rebound to the ligand in the *cis* position with respect to the amine nitrogen of TPA, as a result of the different bond strengths [234]. However, it is noteworthy that the rebound reactivity/selectivity of low-weight synthetic complexes can be considerably influenced by radical escape from the solvent cage and its reaction with other species in solution [235].

In certain cases, an initial C–H abstraction may be followed by the attack of a vicinal C–H bond, furnishing a desaturated product. Intrinsic factors directing the chemoselectivity of OH rebound vs. desaturation by Fe^{IV}–oxo complexes have been studied by Usharani et al. [236], who found that this preference depends on the substrate (C–H bond strength, radical delocalization, etc.) and on the oxidant as well (spin state, orbital structure). They also highlighted that the preferences for the σ/π channels for the second hydrogen abstraction by Fe^{III}–OH are opposite to those for the first one by Fe^{IV}=O. Nevertheless, substrate positioning and conformational issues remain crucial, and often difficult to accurately predict. While theory could give an adequate explanation for the desaturation in a P450 isozyme through the modulation of Fe–OH conformations via hydrogen bonds [237], it had only a partial success in explaining the desaturation over epimerization/hydroxylation selectivity in the α-KG-NHFe carbapenem synthase [92]. Besides substrate positioning, oxidant positioning might be a viable strategy of Nature as well. In this respect, our study on the $NHFe_2$ Δ^9D suggested that a diiron center can be poised in a way that the first C–H abstraction generates an Fe^{IV}=O moiety suitably aligned for a second C–H abstraction on the neighboring carbon atom [85].

Besides these prominent and complex cases, DFT calculations could identify key electronic factors favoring certain reaction outcomes in several further systems. In IPNS, a hydrogen bond from the substrate amide group was found to drive the Fe^{II}–OOH intermediate toward heterolytic cleavage instead of nucleophilic attack, allowing oxidase instead of oxygenase reactivity [238]. A study on a functional model complex of intradiol-cleaving catechol dioxygenase identified the orbital interactions, and the resulting geometric requirements, behind the preference for intradiol cleavage [104]. Presence or absence of an electron transfer concomitantly with a proton transfer was reported to be responsible for the drastically different products of HEPD when presented with 2- or 1-hydroxyethylphosphonate substrates [168]. The inability to bind O_2 was found to be the reason why CDO does not convert selenocysteine into the corresponding seleninic acid [114]. In dimanganese class Ib ribonucleotide reductase, the rate by which the H_2O_2 oxidant is supplied seems to be of key importance in the selectivity toward the native tyrosyl radical generation instead of the possible catalase activity [239].

Regioselectivity

Discrimination among chemically similar functional groups is a task routinely accomplished by the enzymes and still often challenging for synthetic catalysts. Not surprisingly, intrinsic factors often play a lesser role in this field. For example, in a joint mass spectrometric and computational study of biomimetic non-heme Fe^{IV}–oxo complexes, it was found that the preference toward specific aliphatic hydroxylation channels is governed only by proximity effects [240]. An in silico mutagenesis study using MD and QM/MM techniques could identify several amino acids in rabbit 15-lipoxygenase-1 that are responsible for selective hydroperoxidation at C13 and hindering it at C9, obviously the result of steric accessibility (see Fig. 6 for the general lipoxygenase mechanism) [241]. In the reaction catalyzed by prolyl-4-hydroxylase, it was furthermore revealed that the C–H bond broken in the enzyme is actually stronger than those in the 3 and 5 positions, and interactions with second-sphere residues were responsible for the exclusive selectivity contradicting thermodynamic preferences [187].

As seen in the above examples, computations could help reveal important factors behind selectivity in many cases. Nevertheless, one has to keep in mind the possible pitfalls. In our Δ^9D study [85], we revealed that most DFT functionals erroneously predict hydroxylation instead of desaturation due to wrong electron distribution (see also Sect. 3.2.4), pinpointing the need for accurate electronic structure description in selectivity studies. The accurate treatment of environment effects (including solvation) is of

paramount importance, particularly when highly charged active species are investigated [242].

Conclusions

In this minireview, we attempted to highlight the sheer complexity of the NHFe and $NHFe_2$ chemistry and at the same time briefly review the latest progress in theoretical methods of bioinorganic chemistry. We tried to emphasize that the concerted progress on both theoretical and experimental side is a conditio sine qua non for future understanding, exploration and utilization of $NHFe_{(2)}$ systems. This was illustrated on selected examples, including oxidative transformations that are—if uncatalyzed—energetically very difficult and as such require enzymes that use highly reactive intermediates along their catalytic cycles. What we consider as the most fascinating and attractive phenomenon is the fact that despite the strong oxidative power of such intermediates, the NHFe and $NHFe_2$ enzymes perform catalysis with high selectivities. Finally, we are of the opinion that further development of multireference wave function methods is needed to have a solid theoretical basis for benchmarking computationally efficient and easy-to-use DFT methods.

Note added in proof After this paper had been accepted, a recent work of Wójcik et al. (J. Phys. Chem. A, 2016, 120, 1261) came to our attention. Their extensive computational analysis on α-KG-dependent O_2 activation speaks in favor of the S = 2/S = 3 pathways and suggests that BP86 + 10 %HF erroneously over stabilizes the S = 1 Fe(IV)-peroxide adduct.

Acknowledgments The project was supported by the Grant Agency of the Czech Republic (Grants Nos. 15-10279Y, 14-31419S, and 15-19143S), Hungarian Scientific Research Fund (OTKA PD-108955), COST project CM1305 (ECOSTBio) and institutional support RVO 61388963 (CAS). MS also thanks the Czech Academy of Sciences for the Purkyně fellowship.

References

1. Williams RJP, Fraústo da Silva JJR (2000) Coord Chem Rev 200–202:247–348
2. Poulos TL (2014) Chem Rev 114:3919–3962
3. Zheng L, Cash VL, Flint DH, Dean DR (1998) J Biol Chem 273:13264–13272
4. Broderick JB, Duffus BR, Duschene KS, Shepard EM (2014) Chem Rev 114:4229–4317
5. Solomon EI, Brunold TC, Davis MI, Kemsley JN, Lee SK, Lehnert N, Neese F, Skulan AJ, Yang YS, Zhou J (2000) Chem Rev 100:235–350
6. Solomon EI, Light KM, Liu LV, Srnec M, Wong SD (2013) Acc Chem Res 46:2725–2739
7. Blomberg MRA, Borowski T, Himo F, Liao R-L, Siegbahn PEM (2014) Chem Rev 114:3601–3658
8. Nam W (2007) Acc Chem Res 40:522–531
9. Oloo WN, Que L Jr (2015) Acc Chem Res 48:2612–2621
10. Friedle S, Reisner E, Lippard SJ (2010) Chem Soc Rev 39:2768–2779
11. Liu LV, Hong S, Cho J, Nam W, Solomon EI (2013) J Am Chem Soc 135:3286–3299
12. Swart M, Costas M (eds) (2016) Spin states in biochemistry and inorganic chemistry: influence on structure and reactivity. Wiley, UK
13. Johansson AJ, Blomberg MRA, Siegbahn PEM (2008) J Chem Phys 129:154301
14. Rokob TA, Srnec M, Rulíšek L (2012) Dalton Trans 41:5754–5768
15. Neese F (2009) Coord Chem Rev 253:526
16. England J, Bigelow JO, Van Heuvelen KM, Farquhar ER, Martinho M, Meier KK, Frisch JR, Münck E, Que L Jr (2014) Chem Sci 5:1204–1215
17. Light KM, Hangasky JA, Knapp MJ, Solomon EI (2013) J Am Chem Soc 135:9665
18. Biswas AN, Puri M, Meier KK, Oloo WN, Rohde GT, Bominaar EL, Münck E, Que L Jr (2015) J Am Chem Soc 137:2428
19. Bochevarov AD, Li J, Song WJ, Friesner RA, Lippard SJ (2011) J Am Chem Soc 133:7384–7397
20. Bonnot F, Molle T, Ménage S, Moreau Y, Duval S, Favaudon V, Levin-Houée C, Nivière V (2012) J Am Chem Soc 134:5120
21. Diebold AR, Straganz GD, Solomon EI (2011) J Am Chem Soc 133:15979–15991
22. Jayapal P, Ansari A, Rajaraman G (2015) Inorg Chem 54:11077
23. Srnec M, Rokob TA, Schwartz JK, Kwak Y, Rulíšek L, Solomon EI (2012) Inorg Chem 51:2806
24. Chachiyo T, Rodriguez JH (2012) Dalton Trans 41:995
25. Harris TV, Morokuma K (2013) Inorg Chem 52:8551
26. Kwak Y, Jiang W, Dassama LMK, Park K, Bell CB III, Liu LV, Wong SD, Saito M, Kobayashi Y, Kitao S, Seto M, Yoda Y, Alp EE, Zhao J, Bollinger JM Jr, Krebs C, Solomon EI (2013) J Am Chem Soc 135:17573
27. Hirao H, Morokuma K (2010) J Phys Chem Lett 1:901
28. Wörsdörfer B, Conner DA, Yokoyama K, Livada J, Seyedsayamdost M, Jiang W, Silakov A, Stubbe J, Bollinger JM Jr, Krebs C (2013) J Am Chem Soc 135:8585
29. Light KM, Yamanaka Y, Odaka M, Solomon EI (2015) Chem Sci 6:6280
30. Diebold AR, Brown-Marshall CD, Neidig ML, Brownlee JM, Moran GR, Solomon EI (2011) J Am Chem Soc 133:18148–18160
31. McQuilken AC, Ha Y, Sutherlin KD, Siegler MA, Hodgson KO, Hedman B, Solomon EI, Jameson GNL, Goldberg DP (2013) J Am Chem Soc 135:14024
32. Gutman CT, Guzei IA, Brunold TC (2013) Inorg Chem 52:8909
33. Sandala GM, Hopmann KH, Ghosh A, Noodleman L (2011) J Chem Theory Comput 7:3232
34. Pápai M, Vankó G (2013) J Chem Theory Comput 9:5004
35. Borgogno A, Rastrelli F, Bagno A (2015) Chem Eur J 21:12960
36. Roemelt M, Maganas D, DeBeer S, Neese F (2013) J Chem Phys 138:204101
37. Pollock CJ, Debeer S (2011) J Am Chem Soc 133:5594
38. Chandrasekaran P, Stieber SCE, Collins TJ, Que L Jr, Neese F, DeBeer S (2011) Dalt Trans 40:11070
39. Lee N, Petrenko T, Bergmann U, Neese F, Debeer S (2010) J Am Chem Soc 132:9715

40. Sun N, Liu LV, Dey A, Villar-Acevedo G, Kovacs JA, Darensbourg MY, Hodgson KO, Hedman B, Solomon EI (2011) Inorg Chem 50:427
41. Sun N, Dey A, Xiao Z, Wedd AG, Hodgson KO, Hedman B, Solomon EI (2010) J Am Chem Soc 132:12639
42. Park K, Bell CB III, Liu LV, Wang D, Xue G, Kwak Y, Wong SD, Light KM, Zhao J, Alp EE, Yoda Y, Saito M, Kobayashi Y, Ohta T, Seto M, Que L Jr, Solomon EI (2013) Proc Natl Acad Sci 110:6275
43. Park K, Tsugawa T, Furutachi H, Kwak Y, Liu LV, Wong SD, Yoda Y, Kobayashi Y, Saito M, Kurokuzu M, Seto M, Suzuki M, Solomon EI (2013) Angew Chem Int Ed 52:1294
44. Wong SD, Srnec M, Matthews ML, Liu LV, Kwak Y, Park K, Bell CB III, Alp EE, Zhao J, Yoda Y, Kitao S, Seto M, Krebs C, Bollinger JM Jr, Solomon EI (2013) Nature 499:320–323
45. Liu LV, Bell CB III, Wong SD, Wilson SA, Kwak Y, Chow MS, Zhao J, Hodgson KO, Hedman B, Solomon EI (2010) Proc Natl Acad Sci 107:22419–22424
46. Wong SD, Bell CB III, Liu LV, Kwak Y, England J, Alp EE, Zhao J, Que L Jr, Solomon EI (2011) Angew Chem Int Ed 50:3215
47. Park K, Solomon EI (2014) Can J Chem 92:975
48. Han WG, Noodleman L (2010) Theor Chem Acc 125:305
49. Taylor PR (1992) In: Roos BO (ed) Lecture notes in quantum chemistry, vol 58. Springer, Berlin
50. Hampel C, Werner HJ (1996) J Chem Phys 104:6286–6297
51. Neese F, Wennmohs F, Hansen A (2009) J Chem Phys 130:18
52. Eriksen JJ, Baudin P, Ettenhuber P, Kristensen K, Kjærgaard T, Jørgensen P (2015) J Chem Theory Comput 11:2984–2993
53. Dieterich JM, Werner HJ, Mata RA, Metz S, Thiel W (2010) J Chem Phys 132:035101
54. Neese F, Hansen A, Liakos DG (2009) J Chem Phys 131:064103
55. Kowalski K, Piecuch P (2000) J Chem Phys 113:5644–5652
56. Cramer CJ, Włoch M, Piecuch P, Puzzarini C, Gagliardi L (2006) J Phys Chem A 110:1991–2004
57. Roos BO, Veryazov V, Conradie J, Taylor PR, Ghosh A (2008) J Phys Chem B 112:14099–14102
58. Chen H, Ikeda-Saito M, Shaik S (2008) J Am Chem Soc 130:14778–14790
59. Nemukhin AV, Grigorenko BL, Topol IA, Burt SK (2006) Int J Quantum Chem 106:2184–2190
60. Malmqvist P-Å, Pierloot K, Shahi ARM, Cramer CJ, Gagliardi L (2008) J Chem Phys 128:204109
61. Fleig T, Olsen J, Visscher L (2003) J Chem Phys 119:2963–2971
62. Ma D, Li Manni G, Gagliardi L (2011) J Chem Phys 135:044128
63. White SR (1992) Phys Rev Lett 69:2863–2866
64. Legeza Ö, Noack R, Sólyom J, Tincani L (2008) In: Fehske H, Schneider R, Weibe A (eds) Computational many-particle physics, vol 739., Lecture notes in physics, Springer, Berlin
65. Marti KH, Reiher M (2010) Z Phys Chem 224:583–599
66. Chan GKL, Sharma S (2011) Annu Rev Phys Chem 62:465–481
67. Kurashige Y (2014) Mol Phys 112:1485–1494
68. Yanai T, Kurashige Y, Mizukami W, Chalupský J, Lan TN, Saitow M (2015) Int J Quantum Chem 115:283–299
69. Kurashige Y, Chan GKL, Yanai T (2013) Nat Chem 5:660–666
70. Sharma S, Sivalingam K, Neese F, Chan GKL (2014) Nature Chem 6:927–933
71. Stein CJ, Reiher M (2016) arXiv:1602.03835 [physics.chem-ph]
72. Neuscamman E, Yanai T, Chan GKL (2010) J Chem Phys 132:024106
73. Kurashige Y, Chalupský J, Lan TN, Yanai T (2014) J Chem Phys 141:174111
74. Yanai T, Kurashige Y, Neuscamman E, Chan GKL (2010) J Chem Phys 132:024105
75. Saitow M, Kurashige Y, Yanai T (2013) J Chem Phys 139:044118
76. Saitow M, Kurashige Y, Yanai T (2015) J Chem Theory Comput 11:5120–5131
77. Miralles J, Castell O, Caballol R, Malrieu JP (1993) Chem Phys 172:33–43
78. Neese F (2003) J Chem Phys 119:9428–9443
79. Pierloot K (2001) In: Cundari TR (ed) Computational organometallic chemistry. Marcel Dekker, New York
80. Ghigo G, Roos BO, Malmqvist PA (2004) Chem Phys Lett 396:142–149
81. Srnec M, Wong SD, England J, Que L Jr, Solomon EI (2012) Proc Natl Acad Sci 109:14326–14331
82. Delcey MG, Pierloot K, Phung QM, Vancoillie S, Lindh R, Ryde U (2014) Phys Chem Chem Phys 16:7927–7938
83. Radoń M, Broclawik E, Pierloot K (2010) J Phys Chem B 114:1518–1528
84. Ye S, Xue G, Krivokapic I, Petrenko T, Bill E, Que L Jr, Neese F (2015) Chem Sci 6:2909–2921
85. Chalupský J, Rokob TA, Kurashige Y, Yanai T, Solomon EI, Rulíšek L, Srnec M (2014) J Am Chem Soc 136:15977–15991
86. Neese F (2006) J Am Chem Soc 128:10213–10222
87. Neese F (2004) J Phys Chem Solids 65:781–785
88. Andrikopoulos PC, Michel C, Chouzier S, Sautet P (2015) ACS Catal 5:2490–2499
89. Bím D, Rulíšek L, Srnec M (2016) J Phys Chem Lett 7:7–13
90. Light KM, Hangasky JA, Knapp MJ, Solomon EI (2014) Dalton Trans 43:1505–1508
91. Cortopassi WA, Simion R, Honsby CE, França TCC, Paton RS (2015) Chem Eur J 21:18983–18992
92. Ma G, Zhu W, Su H, Cheng N, Liu Y (2015) ACS Catal 5:5556–5566
93. Quesne MG, Latifi R, Gonzalez-Ovalle LE, Kumar D, de Visser SP (2014) Chem Eur J 20:435–446
94. Ye S, Riplinger C, Hansen A, Krebs C, Bollinger JM, Neese F (2012) Chem Eur J 18:6555–6567
95. Meier KK, Rogers MS, Kovaleva EG, Mbughuni MM, Bominaar EL, Lipscomb JD, Münck E (2015) Inorg Chem 54:10269–10280
96. Dong G, Lai W (2014) J Phys Chem B 118:1791–1798
97. Dong G, Shaik S, Lai W (2013) Chem Sci 4:3624–3635
98. Christian GJ, Ye S, Neese F (2012) Chem Sci 3:1600–1611
99. Brkić H, Kovačević B, Tomić S (2015) Mol BioSyst 11:898–907
100. Borowski T, Wójcik A, Miłaczewska A, Georgiev V, Blomberg MRA, Siegbahn PEM (2012) J Biol Inorg Chem 17:881–890
101. Borowski T, Georgiev V, Siegbahn PEM (2010) J Mol Model 16:1673–1677
102. Roy S, Kästner J (2016) Angew Chem Int Ed 55:1168–1172
103. Jastrzebski R, Quesne MG, Weckhuysen BM, de Visser SP, Bruijnincx PCA (2014) Chem Eur J 20:15686–15691
104. Georgiev V, Noack H, Borowski T, Blomberg MRA, Siegbahn PEM (2010) J Phys Chem B 114:5878–5885
105. Wójcik A, Borowski T, Broclawik E (2011) Catal Today 169:207–216
106. Attia AAAA, Cioloboc D, Lupan A, Silaghi-Dumitrescu R (2013) J Biol Inorg Chem 18:95–101
107. Surawatanawong P, Tye JW, Hall MB (2010) Inorg Chem 49:188–192
108. Dey A, Solomon EI (2010) Inorg Chim Acta 363:2762–2767
109. Tremey E, Bonnot F, Moreau Y, Berthomieu C, Desbois A, Favaudon V, Blondin G, Houée-Levin C, Nivière V (2013) J Biol Inorg Chem 18:815–830
110. Sit PH-L, Migliore A, Ho M-H, Klein ML (2010) J Chem Theory Comput 6:2896–2909
111. Kumar D, Thiel W, De Visser SP (2011) J Am Chem Soc 133:3869–3882

112. Kumar D, Sastry GN, Goldberg DP, De Visser SP (2012) J Phys Chem A 116:582–591
113. Che X, Gao J, Zhang D, Liu C (2012) J Phys Chem A 116:5510–5517
114. Blaesi EJ, Gardner JD, Fox BG, Brunold TC (2013) Biochemistry 52:6040–6051
115. Che X, Gao J, Liu Y, Liu C (2013) J Inorg Biochem 122:1–7
116. Olsson E, Martinez A, Teigen K, Jensen VR (2011) Chem Eur J 17:3746–3758
117. Haahr LT, Jensen KP, Boesen J, Christensen HEM (2010) J Inorg Biochem 104:136–145
118. Olsson E, Martinez A, Teigen K, Jensen VR (2010) Eur J Inorg Chem 3:351–356
119. Du L, Gao J, Liu Y, Liu C (2012) J Phys Chem B 116:11837–11844
120. Hirao H, Morokuma K (2010) J Am Chem Soc 132:17901–17909
121. Borowski T, Brocławik E (2003) J Phys Chem B 107:4639
122. Bushnell EAC, Jamil R, Gauld JW (2013) J Biol Inorg Chem 18:343–355
123. Kawatsu T, Lundberg M, Morokuma K (2011) J Chem Theory Comput 7:390–401
124. Miłaczewska A, Broclawik E, Borowski T (2013) Chem Eur J 19:771–781
125. Wang C, Chang W-C, Guo Y, Huang H, Peck SC, Pandelia ME, Lin G, Liu H-W, Krebs C, Bollinger JM Jr (2013) Science 342:991–995
126. Hirao H (2011) J Phys Chem B 115:11278–11285
127. Roos K, Siegbahn PEM (2011) J Biol Inorg Chem 16:553–565
128. Oloo WN, Meier KK, Wang Y, Shaik S, Münck E, Que L Jr (2014) Nat Commun 5:3046
129. Wang Y, Janardanan D, Usharani D, Han K, Que L Jr, Shaik S (2013) ACS Catal 3:1334–1341
130. Prat I, Company A, Postils V, Ribas X, Que L Jr, Luis JM, Costas M (2013) Chem Eur J 19:6724–6738
131. Kim YM, Cho KB, Cho J, Wang B, Li C, Shaik S, Nam W (2013) J Am Chem Soc 135:8838–8841
132. Chen H, Cho KB, Lai W, Nam W, Shaik S (2012) J Chem Theory Comput 8:915–926
133. Petit AS, Pennifold RCR, Harvey JN (2014) Inorg Chem 53:6473–6481
134. Hirao H, Li F, Que L Jr, Morokuma K (2011) Inorg Chem 50:6637–6648
135. Nam W (2015) Acc Chem Res 48:2415–2423
136. McDonald AR, Que L Jr (2013) Coord Chem Rev 257:414–428
137. Lundberg M, Borowski T (2013) Cood Chem Rev 257:277–289
138. Shaik S, Hirao H, Kumar D (2007) Acc Chem Res 40:532–542
139. Usharani D, Janardanan D, Li C, Shaik S (2013) Acc Chem Res 46:471–482
140. Srnec M, Wong SD, Solomon EI (2014) Dalton Trans 43:17567–17577
141. Decker A, Rohde J-U, Klinker EJ, Wong SD, Que L Jr, Solomon EI (2007) J Am Chem Soc 129:15983–15996
142. Ye S, Neese F (2011) Proc Natl Acad Sci 108:1228–1233
143. Krebs C, Fujimori DG, Walsh CT, Bollinger JM (2007) Acc Chem Res 40:484–492
144. Neidig ML, Decker A, Choroba OW, Huang F, Kavana M, Moran GR, Spencer JB, Solomon EI (2006) Proc Natl Acad Sci 103:12966–12973
145. Srnec M, Wong SD, Matthews ML, Krebs C, Bollinger M Jr, Solomon EI (2016) J Am Chem Soc 138:5110–5122
146. Wilson SA, Chen J, Hong S, Lee Y-M, Clémancey M, Garcia-Serres R, Nomura T, Ogura T, Latour J-M, Hedman B, Hodgson KO, Nam W, Solomon EI (2012) J Am Chem Soc 134:11791–11806
147. Grapperhaus CA, Mienert B, Bill E, Weyhermüller T, Wieghardt K (2000) Inorg Chem 39:5306–5317
148. Rohde J-U, In J-H, Lim MH, Brennessel WW, Bukowski MR, Stubna A, Münck E, Nam W, Que L Jr (2003) Science 299:1037–1039
149. Buda F, Ensing B, Gribnau MCM, Baerends EJ (2003) Chem Eur J 9:3436–3444
150. Bernasconi L, Louwerse MJ, Baerends EJ (2007) Eur J Inorg Chem 19:3023–3033
151. Michel C, Baerends EJ (2009) Inorg Chem 48:3628–3638
152. England J, Prakash J, Cranswick MA, Mandal D, Guo Y, Münck E, Shaik S, Que L Jr (2015) Inorg Chem 54:7828–7839
153. Mitra M, Nimir H, Demeshko S, Bhat SS, Malinkin SO, Haukka M, Lloret-Fillol J, Lisensky GC, Meyer F, Shteinman AA, Browne WR, Hrovat DA, Richmond MG, Costas M, Nordlander E (2015) Inorg Chem 54:7152–7164
154. Mayer JM (1998) Acc Chem Res 31:441–450
155. de Visser SP (2010) J Am Chem Soc 132:1087–1097
156. Saouma CT, Mayer JM (2014) Chem Sci 5:21–31
157. Karlsson A, Parales JV, Parales RE, Gibson DT, Eklund H, Ramaswamy S (2003) Science 299:1039–1042
158. Neibergall MB, Stubna A, Mekmouche Y, Münck E, Lipscomb JD (2007) Biochemistry 46:8004–8016
159. Chow MS, Liu LV, Solomon EI (2008) Proc Natl Acad Sci 105:13241–13245
160. Chakrabarty S, Austin RN, Deng DY, Groves JT, Lipscomb JD (2007) J Am Chem Soc 129:3514–3515
161. Ferraro DJ, Gakhar L, Ramaswamy S (2005) Biochem Biophys Res Commun 338:175–190
162. Brown CD, Neidig ML, Neibergall MB, Lipscomb JD, Solomon EI (2007) J Am Chem Soc 129:7427–7438
163. Zhu H, Peck SC, Bonnot F, van der Donk WA, Klinman JP (2015) J Am Chem Soc 137:10448–10451
164. Mbughuni MM, Chakrabarti M, Hayden JA, Bominaar EL, Hendrich MP, Münck E, Lipscomb JD (2010) Proc Natl Acad Sci 107:16788–16793
165. Hong S, Sutherlin KD, Park J, Kwon E, Siegler MA, Solomon EI, Nam W (2014) Nat Commun 5:5440
166. Blaesi EJ, Fox BG, Brunold TC (2014) Biochemistry 53:5759–5770
167. Lundberg M, Kawatsu T, Vreven T, Frisch MJ, Morokuma K (2009) J Chem Theory Comput 5:222–234
168. Hirao H, Morokuma K (2011) J Am Chem Soc 133:14550–14553
169. Chung LW, Li X, Hirao H, Morokuma K (2011) J Am Chem Soc 133:20076–20079
170. Sturgeon BE, Burdi D, Chen SX, Huynh BH, Edmondson DE, Stubbe J, Hoffman BM (1996) J Am Chem Soc 118:7551–7557
171. Wörsdörfer B, Lingaraju M, Yennawar NH, Boal AK, Krebs C, Bollinger JM, Pandelia M-E (2013) Proc Natl Acad Sci 110:18874–18879
172. Xing G, Diao Y, Hoffart LM, Barr EW, Prabhu KS, Arner RJ, Reddy CC, Krebs C, Bollinger JM (2006) Proc Natl Acad Sci 103:6130–6135
173. Hirao H, Morokuma K (2009) J Am Chem Soc 131:17206–17214
174. Sastri CV, Lee J, Oh K, Lee YJ, Lee J, Jackson TA, Ray K, Hirao H, Shin W, Halfen JA, Kim J, Que L Jr, Shaik S, Nam W (2007) Proc Natl Acad Sci 104:19181–19186
175. Lacy DC, Gupta R, Stone KL, Greaves J, Ziller JW, Hendrich MP, Borovik AS (2010) J Am Chem Soc 132:12188–12190
176. Kwon E, Cho K-B, Hong S, Nam W (2014) Chem Commun 50:5572–5575
177. Ghosh M, Singh KK, Panda C, Weitz A, Hendrich MP, Collins TJ, Dhar BB, Gupta SS (2014) J Am Chem Soc 136:9524–9527

178. Yosca TH, Rittle J, Krest CM, Onderko EL, Silakov A, Calixto JC, Behan RK, Green MT (2013) Science 342:825–8297
179. Usharani D, Lacy DC, Borovik AS, Shaik S (2013) J Am Chem Soc 135:17090–17104
180. Hammes-Schiffer S, Stuchebrukhov AA (2010) Chem Rev 110:6939–6960
181. Hammes-Schiffer S (2015) J Am Chem Soc 137:8860–8871
182. Wang LP, Van Voorhis TA (2012) J Chem Theory Comput 8:610–617
183. Li JL, Farrokhnia M, Rulíšek L, Ryde U (2015) J Phys Chem B 119:8268–8284
184. Rulíšek L (2013) J Phys Chem C 117:16871–16877
185. Riggs-Gelasco PJ, Price JC, Guyer RB, Brehm JH, Barr EW, Bollinger JM, Krebs C (2004) J Am Chem Soc 126:8108–8109
186. Hoffart LM, Barr EW, Guyer RB, Bollinger JM, Krebs C (2006) Proc Natl Acad Sci 103:14738–14743
187. Karamzadeh B, Kumar D, Sastry GN, de Visser SP (2010) J Phys Chem A 114:13234–13243
188. Mandal D, Ramanan R, Usharani D, Janardanan D, Wang B, Shaik S (2015) J Am Chem Soc 137:722–733
189. Truong TN, Truhlar DG (1990) J Chem Phys 93:1761–1769
190. Duncan WT, Bell RL, Troung TN (1998) J Comput Chem 19:1039–1052
191. Layfield JP, Hammes-Schiffer S (2014) Chem Rev 114:3466–3494
192. Meyer MP, Tomchick DR, Klinman JP (2008) Proc Natl Acad Sci 105:1146–1151
193. Hu S, Sharma SC, Scouras AD, Soudackov AV, Carr CAM, Hammes-Schiffer S, Alber T, Klinman JP (2014) J Am Chem Soc 136:8157–8160
194. Eser BE, Barr EW, Frantom PA, Saleh L, Bollinger JM Jr, Krebs C, Fitzpatrick PF (2007) J Am Chem Soc 129:11334–11335
195. Panay AJ, Lee M, Krebs C, Bollinger JM Jr, Fitzpatrick PF (2011) Biochemistry 50:1928–1933
196. Bassan A, Blomberg MRA, Siegbahn PEM (2003) Chem Eur J 9:106–115
197. Moran GR, Derecskei-Kovacs A, Hillas PJ, Fitzpatrick PF (2000) J Am Chem Soc 122:4535–4541
198. Borowski T, Bassan A, Siegbahn PEM (2004) Biochemistry 43:12331–12342
199. Ye S, Wu X, Wei L, Tang D, Sun P, Bartlam M, Rao Z (2007) J Biol Chem 282:3391–3402
200. Crawford JA, Li W, Pierce BS (2011) Biochemistry 50:10241–10253
201. Cho KB, Shaik S, Nam W (2010) Chem Commun 46:4511–4513
202. England J, Martinho M, Farquhar ER, Frisch JR, Bominaar EL, Münck E, Que L Jr (2009) Angew Chem Int Ed Engl 48:3622–3626
203. England J, Guo Y, Farquhar ER, Young VG Jr, Münck E, Que L Jr (2010) J Am Chem Soc 132:8635–8644
204. Bigi JP, Harman WH, Lassalle-Kaiser B, Robles DM, Stich TA, Yano J, Britt RD, Chang CJ (2012) J Am Chem Soc 134:1536–1542
205. England J, Guo Y, Van Heuvelen KM, Cranswick MA, Rohde GT, Bominaar EL, Münck E, Que L Jr (2011) J Am Chem Soc 133:11880–11883
206. Wang D, Ray K, Collins MJ, Farquhar ER, Frisch JR, Gomez L, Jackson TA, Kerscher M, Waleska A, Comba P, Costas M, Que L Jr (2013) Chem Sci 4:282–291
207. Hong S, Lee Y-M, Cho K-B, Sundaravel K, Cho J, Kim MJ, Shin W, Nam W (2011) J Am Chem Soc 133:11876–11879
208. Hong S, So H, Yoon H, Cho K-B, Lee Y-M, Fukuzumi S, Nam W (2013) Dalton Trans 42:7842–7845
209. Fukuzumi S, Morimoto Y, Kotani H, Naumov P, Lee Y-M, Nam W (2010) Nat Chem 2:756–759
210. Morimoto Y, Kotani H, Park J, Lee YM, Nam W, Fukuzumi S (2011) J Am Chem Soc 133:403–405
211. Park J, Morimoto Y, Lee Y, Nam W, Fukuzumi S (2011) J Am Chem Soc 133:5236–5239
212. Park J, Morimoto Y, Lee YM, Nam W, Fukuzumi S (2012) J Am Chem Soc 134:3903–3911
213. Swart M (2013) Chem Commun 49:6650–6652
214. Prakash J, Rohde GT, Meier KK, Jasniewski AJ, Van Hauvelen KM, Munck E, Que L Jr (2015) J Am Chem Soc 137:3478–3481
215. Widger LR, Davies CG, Yang T, Siegler MA, Troeppner O, Jameson GNL, Ivanović-Burmazović I, Goldberg DP (2014) J Am Chem Soc 136:2699–2702
216. Sahu S, Widger LR, Quesne MG, de Visser SP, Matsumura H, Moënne-Loccoz P, Siegler MA, Goldberg DP (2013) J Am Chem Soc 135:10590–10593
217. Bassan A, Blomberg MRA, Siegbahn PEM (2004) J Biol Inorg Chem 9:439–452
218. Tarasev M, Ballou DP (2005) Biochemistry 44:6197–6207
219. Que L Jr, Ho RYN (1996) Chem Rev 96:2607–2624
220. Chen K, Que L Jr (1999) Chem Commun 15:1375–1376
221. Chen K, Que L Jr (2001) J Am Chem Soc 123:6327–6337
222. Ansari A, Kaushik A, Rajaraman G (2013) J Am Chem Soc 135:4235–4249
223. Park MJ, Lee J, Sun Y, Kim J, Nam W (2006) J Am Chem Soc 128:2630–2634
224. Seo MS, Kamachi T, Kuono T, Murata K, Park MJ, Yoshizawa K, Nam W (2007) Angew Chem Int Ed Engl 46:2291–2294
225. Jiang Y, Telser J, Goldberg DP (2009) Chem Commun 6828–6830
226. Cho J, Jeon S, Wilson SA, Liu LV, Kang EA, Braymer JJ, Lim MH, Hedman B, Hodgson KO, Valentine JS, Solomon EI, Nam W (2011) Nature 478:502–505
227. Rat S, Ménage S, Thomas F, Nivière V (2014) Chem Commun 50:14213–14216
228. Wójcik A, Broclawik E, Siegbahn PEM, Borowski T (2012) Biochemistry 51:9570–9580
229. Wójcik A, Broclawik E, Siegbahn PEM, Lundberg M, Moran G, Borowski T (2014) J Am Chem Soc 136:14472–14485
230. De Visser SP, Latifi R, Tahsini L, Nam W (2011) Chem Asian J 6:493–504
231. Matthews ML, Neumann CS, Miles LA, Grove TL, Booker SJ, Krebs C, Walsh CT, Bollinger JM Jr (2009) Proc Natl Acad Sci 106:17723–17728
232. Borowski T, Noack H, Radoń M, Zych K, Siegbahn PEM (2010) J Am Chem Soc 132:12887–12898
233. Martinie RJ, Livada J, Chang W, Green MT, Krebs C, Bollinger JM Jr, Silakov A (2015) J Am Chem Soc 137:6912–6919
234. Quesne MG, De Visser SP (2012) J Biol Inorg Chem 17:841–852
235. Puri M, Biswas AN, Fan R, Guo Y, Que L Jr (2016) J Am Chem Soc 138:2484–2487
236. Usharani D, Janardanan D, Shaik S (2011) J Am Chem Soc 133:176–179
237. Ji L, Faponle AS, Quesne MG, Sainna MA, Zhang J, Franke A, Kumar D, van Eldik R, Liu W, de Visser SP (2015) Chem Eur J 21:9083–9092
238. Brown-Marshall CD, Diebold AR, Solomon EI (2010) Biochemistry 49:1176–1182
239. Roos K, Siegbahn PEM (2013) Inorg Chem 52:4173–4184
240. Mas-Ballesté R, McDonald AR, Reed D, Usharani D, Schyman P, Milko P, Shaik S, Que L Jr (2012) Chem Eur J 18:11747–11760
241. Suardíaz R, Masgrau L, Lluch JM, González-Lafont À (2014) ChemPhysChem 15:4049–4054
242. Postils V, Company A, Solà M, Costas M, Luis JM (2015) Inorg Chem 54:8223–8236